THE DISTRIBUTION OF SATELLITES AROUND MASSIVE GALAXIES AT $1 < Z < 3$ IN ZFOURGE/CANDELS: DEPENDENCE ON STAR FORMATION ACTIVITY[*]

Lalitwadee Kawinwanichakij[1†], Casey Papovich[1], Ryan F. Quadri[1,2,3,4], Kim-Vy H. Tran[1], Lee R. Spitler[5,6], Glenn G. Kacprzak[7,8], Ivo Labbé[9], Caroline M. S. Straatman[9], Karl Glazebrook[7], Rebecca Allen[6,7], Michael Cowley[5], Romeel Davé[10,11,12], Avishai Dekel[13], Henry C. Ferguson[14], W. G Hartley[15,16], Anton M. Koekemoer[14], David C. Koo[17], Yu Lu[18], Nicola Mehrtens[1], Themiya Nanayakkara[7], S. Eric Persson[3], Glen Rees[5], Brett Salmon[1], Vithal Tilvi[1], Adam R. Tomczak[1], and Pieter van Dokkum[19]

Draft version June 6, 2018

ABSTRACT

We study the statistical distribution of satellites around star-forming and quiescent central galaxies at $1 < z < 3$ using imaging from the FourStar Galaxy Evolution Survey (ZFOURGE) and the Cosmic Assembly Near-IR Deep Extragalactic Legacy Survey (CANDELS). The deep near-IR data select satellites down to $\log(M/M_\odot) > 9$ at $z < 3$. The radial satellite distribution around centrals is consistent with a projected NFW profile. Massive quiescent centrals, $\log(M/M_\odot) > 10.78$, have ∼2 times the number of satellites compared to star-forming centrals with a significance of 2.7σ even after accounting for differences in the centrals' stellar-mass distributions. We find no statistical difference in the satellite distributions of intermediate-mass quiescent and star-forming centrals, $10.48 < \log(M/M_\odot) < 10.78$. Comparing to the Guo et al. (2011) semi-analytic model, the excess number of satellites indicates that quiescent centrals have halo masses 0.3 dex larger than star-forming centrals, even when the stellar-mass distributions are fixed. We use a simple toy model that relates halo mass and quenching, which roughly reproduces the observed quenched fractions and the differences in halo mass between star-forming and quenched galaxies only if galaxies have a quenching probability that increases with halo mass from ∼0 for $\log(M_h/M_\odot)$ ∼11 to ∼1 for $\log(M_h/M_\odot)$ ∼13.5. A single halo-mass quenching threshold is unable to reproduce the quiescent fraction and satellite distribution of centrals. Therefore, while halo quenching may be an important mechanism, it is unlikely to be the only factor driving quenching. It remains unclear why a high fraction of centrals remain star-forming even in relatively massive halos.

Keywords: galaxies: evolution — galaxies: high-redshift — galaxies: halos — galaxies: statistics

*This paper includes data gathered with the 6.5 meter Magellan Telescopes located at Las Campanas Observatory, Chile.

[1] George P. and Cynthia W. Mitchell Institute for Fundamental Physics and Astronomy, Department of Physics and Astronomy,Texas A&M University, College Station, TX 77843
[2] Mitchell Astronomy Fellow
[3] Carnegie Observatories, Pasadena, CA 91101, USA
[4] Hubble Fellow
[5] Department of Physics and Astronomy, Faculty of Sciences, Macquarie University, Sydney, NSW 2109, Australia
[6] Australian Astronomical Observatories, PO Box 915, North Ryde NSW 1670, Australia
[7] Centre for Astrophysics and Supercomputing, Swinburne University, Hawthorn, VIC 3122, Australia
[8] Australian Research Council Super Science Fellow
[9] Leiden Observatory, Leiden University, P.O. Box 9513, 2300 RA Leiden, The Netherlands
[10] University of the Western Cape, Bellville, Cape Town 7535, South Africa
[11] South African Astronomical Observatories, Observatory, Cape Town 7925, South Africa
[12] African Institute for Mathematical Sciences, Muizenberg, Cape Town 7945, South Africa
[13] Center for Astrophysics and Planetary Science, Racah Institute of Physics, The Hebrew University, Jerusalem 91904, Israel
[14] Space Telescope Science Institute, 3700 San Martin Drive, Baltimore, MD 21218, USA
[15] School of Physics and Astronomy, University of Nottingham, Nottingham NG7 2RD, UK
[16] Institute for Astronomy, ETH Zurich, Wolfgang-Pauli-Strasse 27, CH-8093 Zurich,Switzerland
[17] University of California Observatories/Lick Observatory, Department of Astronomy and Astrophysics, University of California, Santa Cruz, CA 95064, USA
[18] Kavli Institute for Particle Astrophysics & Cosmology, 452 Lomita Mall, Stanford, CA 94305, USA
[19] Department of Astronomy, Yale University, New Haven, CT 06520, USA
† kawinwanichakij@physics.tamu.edu

1. INTRODUCTION

One of the fundamental goals in studying galaxy formation and evolution is to understand the relationship between galaxies and their host dark matter halos. In ΛCDM models galaxies grow hierarchically, and we expect to see the signatures of such growth in satellite galaxies, which trace the accreted dark-matter sub-halos. The distribution of satellite galaxies can be used as a tracer of the overall mass distribution of the parent halo and provides constraints on the halo mass. Therefore, investigating the distribution of satellites provides a means to study how properties of host galaxies (such as stellar mass and star formation activity) are related to the mass of their dark matter halos.

The distribution of satellite galaxies provides constraints that are independent of other techniques that use correlation functions, galaxy-galaxy lensing, adundance matching, and kinematics to study how the dark matter masses relate to galaxy observables (e.g. Vader & Sandage 1991; Zehavi et al. 2002; Madore et al. 2004; Mandelbaum et al. 2006; Masjedi et al. 2006; Gavazzi et al. 2007; Wake et al. 2008; Conroy & Wechsler 2009; Drory et al. 2009;

Behroozi et al. 2010; Hartley et al. 2010, 2013; More et al. 2011). Several studies show that the distribution of satellite galaxies follows a Navarro, Frenk, & White (1996) profile (NFW-profile), and this can be used to measure the mass distribution and scale size of the dark matter halo (Nierenberg et al. 2011, 2012; Tal et al. 2012, 2013; Wang & White 2012; Watson et al. 2012; Wang et al. 2014).

Studying the distribution of satellite galaxies is expected to provide particular insight into galaxy evolution for massive galaxies. Growing observational evidence suggests that massive ($> 10^{11}$ M$_\odot$), quiescent galaxies (those lacking substantial star-formation) have grown primarily in their outer regions through the accretion of small satellites since $z \sim 2$ (e.g. van Dokkum et al. 2010; McLure et al. 2012; Greene et al. 2012, 2013). This is consistent with the results from hydrodynamical simulations, which have reproduced the observed size and mass growth of massive elliptical galaxies by stellar accretion from minor mergers (Naab et al. 2007, 2009; Oser et al. 2010, 2012; Hilz et al. 2013).

Tal et al. (2012) use a statistical background subtraction to measure the radial number-density profiles of satellites around local luminous red galaxies (LRGs). They show that the best fit NFW+Sérsic model of the derived satellites profile results in a total dark-to-baryonic mass ratio in agreement with the weak-lensing result from Mandelbaum et al. (2006) for massive early type galaxies. Tal et al. (2013) extend this technique to massive galaxies out to $z \sim 2$ and show that the radial number density profile of satellite galaxies has not evolved significantly since $z = 1.6$, suggesting a balance between mergers and accretion of new satellites.

Recently, Hartley et al. (2014) have used a similar method to study the properties of satellites of centrals out to $z < 1.9$ using data in the UKIDSS UDS, albeit with a higher mass limit for satellites, $\log M/M_\odot > 9.7$.

The technique used by Tal et al. (2012, 2013) requires statistically isolating satellites from unassociated galaxies along the line of sight. Surveys with homogeneous multiwavelength photometry provide photometric redshift information on faint galaxies, which is useful to identify satellites around more distant galaxies as shown by Tal et al (2013). This statistical technique has an advantage over methods using spectroscopic redshifts, as the latter are observationally prohibitive for all but the brightest satellites and very costly in telescope time.

At $z > 1$, growing evidence shows that massive galaxies are a mix of quiescent and star-forming populations (e.g. Papovich et al. 2006). This is an extension of the well-known bimodality in their color and star-formation activity. At fixed stellar mass, galaxies divide into star-forming galaxies with bluer UV–optical colors and active star formation (forming a "main sequence", e.g., Noeske et al. 2007; Martin et al. 2007), and quiescent galaxies with red colors and low star formation rates compared to their past average (forming a "red sequence", e.g. Bell et al. 2004; Blanton 2006). This bimodality in the galaxy color-mass distribution extends at least out to $z \sim 3$ (Whitaker et al. 2011; Tomczak et al. 2014) and perhaps beyond (Spitler et al. 2014, Straatman et al. 2014). Recent studies of the evolution of the progenitors of local ultra-massive galaxies ($\log (M/M_\odot) \approx 11.8$) at $1 < z < 3$ shows that the contribution of star-

forming galaxies increases at $z > 1$. Understanding why some massive galaxies are quiescent and some are star-forming has important implications for galaxy formation models (e.g. Croton et al. 2006; Martig et al. 2009; Dekel & Birnboim 2006). This may be tied to differences in the galaxies' dark matter halo growth. For this reason, it is of interest to study differences in the satellite distribution of quiescent and star-forming centrals at $1 < z < 3$ because it allows us to trace the dark-matter halos of such objects when the dichotomy in star-formation activity (quiescent versus star-forming) is at its peak for massive galaxies (e.g. Marchesini et al. 2014)

In this work, we use the most recent data from the FourStar Galaxy Evolution Survey (ZFOURGE) and the Cosmic Assembly Near-IR Deep Extragalactic Legacy Survey (CANDELS) to derive the distribution of satellites around massive galaxies at $1 < z < 3$. We study the dependence of the galaxy distribution on the star formation activity of the massive centrals. The outline of this paper is as follows. In § 2 we describe our ZFOURGE/CANDELS dataset and our galaxy sample selection criteria. In § 3 we describe the method for identifying satellites and for measuring the satellite number density profile. In § 4 we discuss how the satellite distribution depends on the stellar mass and star-formation activity of central galaxy. In § 5, we explore why quiescent and star-forming galaxies have differences in their satellite distributions, including a comparison between galaxies in our dataset and those in a semi-analytical model (Guo et al. 2011). In § 6, we present our summary. Throughout, we adopt the following cosmological parameters where appropriate, $H_0 = 70 \,\mathrm{km\,s^{-1}\,Mpc^{-1}}$, $\Omega_m = 0.3$, and $\Omega_\Lambda = 0.7$. For this cosmology, the angular diameter conversion is ≈ 8 kpc arcsec^{-1} and constant within 5% for $1 < z < 3$.

2. DATA AND SAMPLE SELECTION

We use the deep near-IR imaging from ZFOURGE (Straatman et al. in prep[21]), which is composed of three $11' \times 11'$ pointings with coverage in the CDFS (Giacconi et al. 2002), COSMOS (Capak et al. 2007), and UDS (Lawrence et al. 2007). The imaging reaches depths of ~ 26 mag in J_1, J_2, J_3 and ~ 25 mag in H_s, H_l, K_s. A brief description of the filter set is described in detail by Spitler et al. (2012); Tilvi et al. (2013). The medium-band filters from ZFOURGE provide an advantage by sampling the Balmer break at $1 < z < 4$ better than broadband filters alone. We combine the ZFOURGE data with public HST/WFC3 F160W and F125W imaging from CANDELS (Grogin et al. 2011; Koekemoer et al. 2011) in the three fields. As described in Tomczak et al. (2014), we make use of the CANDELS F160W as a detection image to preselect a sample of galaxies at $z < 3$ to low masses (10^9 M$_\odot$).

Photometry is performed in dual-image mode with SExtractor (Bertin & Arnouts 1996) on PSF-matched images. The colors are measured in 0.8″ apertures, and total magnitudes are measured using the AUTO magnitude and applying an aperture correction for the flux falling outside the AUTO aperture.

As described by Tomczak et al. (2014), we estimate the photometric redshifts and rest-frame colors of galax-

ies with EAZY (Brammer et al. 2008). By using the default set of spectral templates derived from the PEGASE models (Fioc & Rocca-Volmerange 1997) and a dust reddened template derived from the Maraston (2005) model to fit the $0.3 - 8\,\mu$m photometry for each galaxy to obtain its photometric redshift. Similarly, we derive stellar masses using Bruzual & Charlot (2003) stellar population models with FAST code (Kriek et al. 2009), assuming exponentially declining star formation histories, solar metallicity, and a Chabrier (2003) initial mass function.

We estimate relative uncertainties in photometric redshifts using the technique described by Quadri & Williams (2010). For our study, the relative errors between the centrals and satellites are paramount, and traditional photometric redshift testing (comparing photometric redshifts to spectroscopic) is infeasible as the satellite galaxies in our sample are typically much fainter than spectroscopic magnitude limits. The underlying principle of the Quadri & Williams technique is that close pairs of galaxies have some probability of being physically associated. In this case, each galaxy provides an independent estimate of the true redshift. Therefore, the distribution of the differences in the photometric redshifts of galaxy pairs can be used to estimate the photometric redshift uncertainties.

We apply this method to derive the distribution of differences between the photometric redshifts of centrals and satellites using the samples defined below (§ 2.1 and § 2.2). From these we find that the typical photometric redshift uncertainty between the centrals and satellites in the COSMOS, CDFS, and UDS fields are $\sigma_z =$ 0.06, 0.05, and 0.08, respectively (where $\sigma_z = \sigma/\sqrt{2}$, and where σ is the width measured from a Gaussian fit to the distribution of pair redshift differences in each field, and the $\sqrt{2}$ accounts for the fact that we take the difference between two independent measurements). These uncertainties translate to $\sigma_z/(1+z) < 2\%$ and 4% for galaxies at $1 < z < 3$ down to 10^9 M$_\odot$.

Throughout, we consider two samples of galaxies, the central galaxies and their satellite galaxies, which are defined in § 2.1 and § 2.2. We denote the stellar masses of the centrals as M_c and the stellar masses of the satellites as M_{sat}. We use N_{sat} throughout to denote the radial number density of satellites around the central galaxies, and correct this quantity for projected field galaxies (§ 3.1).

### 2.1. Selection of Centrals

Our goal is to measure the distribution of satellites around massive galaxies at $1 < z < 3$. We therefore select all galaxies in ZFOURGE with $\log(M_c/M_\odot) > 10.48$ (i.e., $M_c > 3 \times 10^{10}$ M$_\odot$) and photometric redshift $1 < z < 3$ as our sample of central galaxies. We will further consider the subsamples of central galaxies in bins of stellar mass, $10.48 < \log(M_c/M_\odot) < 10.78$ (i.e., $M_c = (3 - 6) \times 10^{10}$ M$_\odot$) and $\log(M_c/M_\odot) > 10.78$ (i.e., $M_c > 6 \times 10^{10}$ M$_\odot$). A summary of number and mean stellar mass of centrals in each of the ZFOURGE field and in each subsample is given in Table 1.

According to the central galaxies selection criteria used by Tal et al. (2013), they consider galaxies as "central" if no other, more massive galaxies are found within a

Table 1
Number and mean stellar masses of quiescent centrals and star-forming centrals in ZFOURGE survey at $1 < z < 3$

Field	$\log(M_c/M_\odot)$	N_c	$\log(M_{c,mean}/M_\odot)$
Quiescent centrals			
COSMOS	10.48–10.78	63	10.61
	> 10.78	67	11.01
CDFS	10.48–10.78	46	10.61
	> 10.78	53	11.02
UDS	10.48–10.78	96	10.61
	> 10.78	70	11.04
Star-forming centrals			
COSMOS	10.48–10.78	85	10.62
	> 10.78	71	11.08
CDFS	10.48–10.78	83	10.62
	> 10.78	52	11.03
UDS	10.48–10.78	87	10.62
	> 10.78	68	10.97
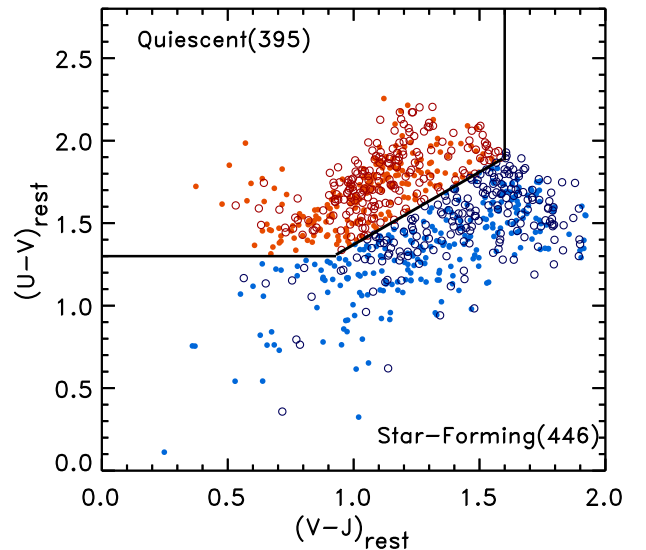
Figure 1. Rest-frame $U - V$ versus $V - J$ color for massive central galaxies in our sample from all three ZFOURGE pointings (COSMOS, CDFS, and UDS) at $1 < z < 3$. The data points show centrals with stellar masses of $10.48 < \log(M_c/M_\odot) < 10.78$ (small filled circles) and $\log(M_c/M_\odot) > 10.78$ (large open circles). The galaxies in the upper left region of the plot (separated by the solid line) are quiescent (red open and filled circles); galaxies outside this region are star forming (blue open and filled circles), using the definition of Williams et al. (2009) and Equation 1. The numbers of quiescent and star-forming centrals are indicated in parentheses in the plot legend. Quiescent and star-forming galaxies each account for approximately half of galaxies population at these masses and redshifts.

projected radius of 500 kpc. Otherwise, they are counted as satellites of their more massive neighbor. We have tested if the projected radial distribution changes if we exclude galaxies from our sample of central galaxies if there are other more massive galaxies within 10 arcsec (about 80 kpc, projected), which is comparable to our derived halo scale radius (described in § 3.2, below). We find that our derived projected radial distribution is not significantly changed. Therefore, we do not apply this isolation criteria to select our central sample. However, this may introduce galaxies which are satellites into our sample of centrals. In § 5.2 we further quantify the effects of the misclassification of centrals and satellites on the

Table 2
Summary of the probabilities p-values comparing the number density of satellites
around quiescent and star-forming centrals at $1 < z < 3$ in the ZFOURGE survey.

Sample (1)	$\log(M_c/M_\odot)$ (2)	N_c(Quiescent) (3)	N_c(Star − forming) (4)	p_{MC} (5)
All centrals	> 10.48	395	446	0.081
	10.48-10.78	205	255	0.478
	> 10.78	190	191	0.002
Fixed in stellar mass	> 10.48	337	337	0.550
	10.48-10.78	195	195	0.985
	> 10.78	142	142	0.004

Note. — (1) Description of samples used, (2) stellar mass of the sample, (3) number of quiescent centrals, (4) number of star-forming centrals, and (5) The probability we derive from our Monte Carlo simulations that we would have obtain a difference between the satellite distributions of the quiescent and star-forming centrals by chance. Low probabilities (p-value) indicate more significant differences in the distributions.

number density of satellites using results from a mock galaxy catalog.

We then consider the subsamples of central galaxies divided by star-formation activity. Williams et al. (2009) show that the $U - V$ and $V - J$ rest-frame colors are able to distinguish reliably between quiescent galaxies with low specific SFRs (sSFR) and star-forming galaxies with high specific SFRs; see also discussion in Whitaker et al. (2011). Galaxies are classified as quiescent if their rest-frame colors satisfy these criteria:

$$U - V > 0.88 \times (V - J) + 0.49$$
$$U - V > 1.3 \qquad (1)$$
$$V - J < 1.6$$

Figure 1 shows the $U - V$ vs. $V - J$ diagram (hereafter UVJ diagram) for the centrals in our ZFOURGE samples. We find that between $1 < z < 3$ the massive centrals (841 in total with $M_c > 3 \times 10^{10}$ $M_\odot$) are roughly evenly divided into quiescent galaxies (47%) and star-forming galaxies (53%) based on their UVJ colors. The numbers of the quiescent and star-forming centrals in each ZFOURGE field and mass subsample are shown in Table 1.

2.2. Selection of Satellites

To identify satellites of the central galaxies in our sample, we build on the statistical background subtraction technique, as discussed in Tal et al. (2012, 2013). We first select all galaxies around each central from our ZFOURGE catalogs that satisfy the following conditions

$$|z_c - z_{sat}| \leq 0.2$$
$$10^9 \ M_\odot \leq M_{sat} < M_c \qquad (2)$$
$$(3)$$

where z_c and z_{sat} are the photometric redshift of the central and satellite, respectively. Similarly, M_c and M_{sat} are the stellar mass of the central and satellite, respectively. Our requirement that $\Delta z = |z_c - z_{sat}| \leq 0.2$ is motivated by our relative photometric uncertainty (σ_z) between centrals and satellites derived above. In each case, the σ_z values for galaxies in each ZFOURGE field are less than about half the $\Delta z \leq 0.2$ requirement in Equation 2, which argues that this selection criterion is appropriate.

The mass-completeness limits for all galaxies in the ZFOURGE sample at $z = 3$ are $\log(M/M_\odot) = 9.3$ (Tomczak et al. 2014). Below these mass limits, we are incomplete for quiescent galaxies, while our sample remains complete for star-forming galaxies down to $\log(M/M_\odot) = 9$. However, in this study, we are comparing the relative number of satellites between quiescent and star-forming centrals, so they have the same relative bias due to incompleteness in satellite detection. Parenthetically, we note that we have also repeated our analysis restricting the centrals to $1 < z < 2$, where incompleteness is less of an issue, and our primary conclusions are unchanged.

We consider the possibility that our samples of quiescent and star-forming centrals have different redshift distributions. For example, it could be plausible that the quiescent centrals tend to have lower redshifts, while star-forming centrals tend to have higher redshift. In this hypothetical case, we might expect more satellites around quiescent galaxies because we can see them to lower mass. We therefore compared the redshift distributions of the different subsampltes. For the intermediate mass star-forming and quiescent centrals ($10.48 < \log(M_c/M_\odot) < 10.78$), there is no difference in their redshift distributions. There is some difference in the redshift distributions between the star-forming and quiescent centrals in the higher mass subsample. However, in § 5.1 we show that this difference does not effect our main results. Therefore, we conclude that the redshift distributions of central galaxies does not affect the relative number of satellites between the star-forming and quiescent samples.

## 3. RADIAL NUMBER DENSITY PROFILES

3.1. Profile derivation

The method to extract a radial distribution of satellites is illustrated in Figure 2, expanding from the method outlined in Tal et al. (2012). For a given projected distance from each central, we measure the number of all galaxies satisfying our definition of satellite in Equation 2. This includes both physically associated galaxies, as well as chance alignments of foreground and background galaxies. We measure the projected radial distribution by binning the distance from those galaxies to central galaxies in logarithmic bins.
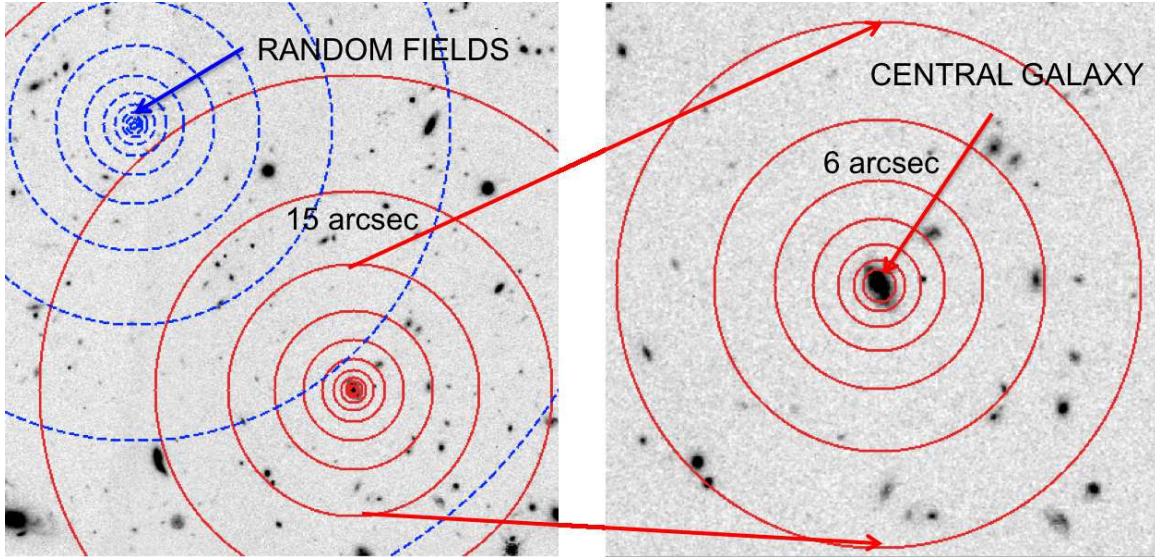
Figure 2. Demonstration of the statistical technique to measure the radial number density profile of satellite galaxies. All galaxies that satisfy the definition of "satellite" in Equation 2 are divided into $\log(r)$ bins around each central (red solid circles) and also around randomly selected positions in the field (blue dashed circles). The number density profile of satellites is then measured from the difference between the satellites measured around the central and those measured in the field. In practice, we use many random fields per each central and calculate the average to infer the statistical distribution of foreground and background galaxies. In this figure we show one random field for illustration only.
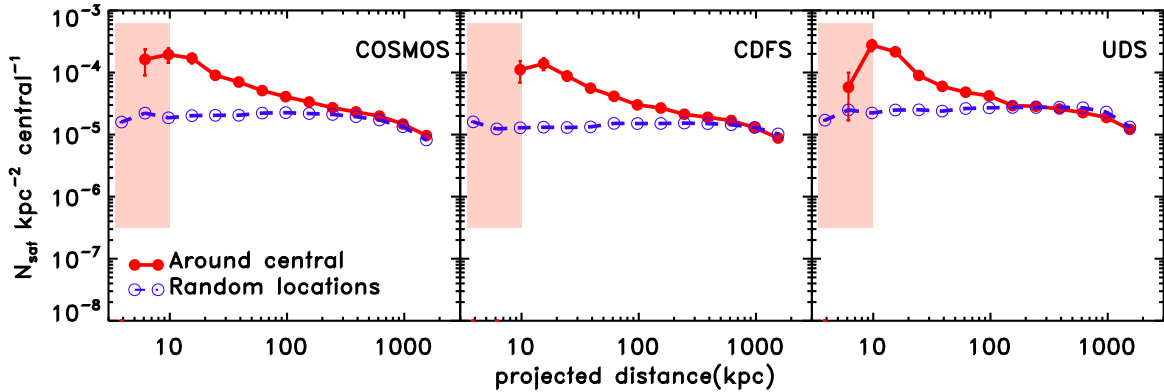
Figure 3. The average projected radial profile of satellites around central galaxies at $1 < z < 3$ with stellar masses of $\log(M_c/M_\odot) > 10.48$ and the field in each pointing of ZFOURGE (COSMOS, CDFS, and UDS). The measured projected distribution of satellites is calculated by subtracting the average random profile (blue lines with open circles) from that measured around the central galaxy profile (red lines with filled circles). The shaded areas show the range of projected distance where satellites are blended with centrals; these we exclude from our analysis. Uncertainties on the random profiles are small compared to the symbol sizes, and are not shown.
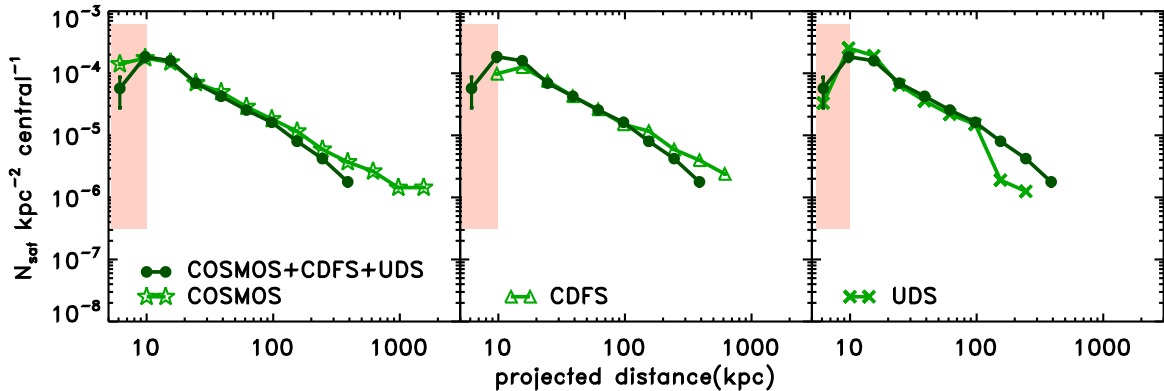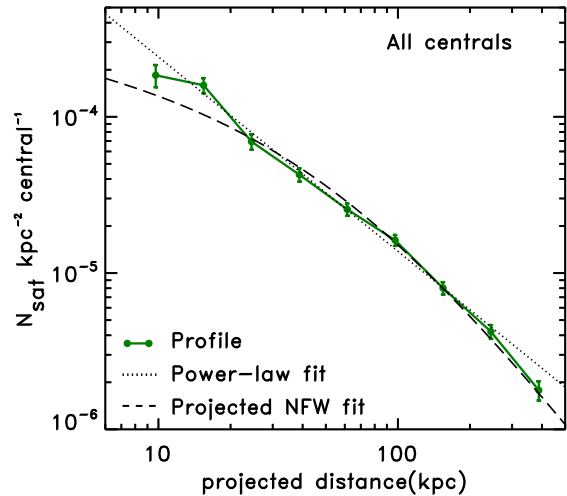

Figure 4. The projected radial profile for central galaxies at $1 < z < 3$ with stellar masses of $\log(M_c/M_\odot) > 10.48$ combined from all ZFOURGE fields (dark green solid line), compared to the profiles of each field separately (light green). In each panel, the combined measurement is the same, where each field shows the result from COSMOS (left panel), CDFS (middle panel), and UDS (right panel). The profile of each field separately is consistent with the combined one at $10 < r/\mathrm{kpc} < 100$, but differences exist at larger projected radii, which we attribute to variations in the background of field galaxies.

We remove the contamination from foreground and background galaxies statistically by repeating the measurements in randomly selected positions within the entire area of the ZFOURGE fields. While we use all centrals, some centrals are near the survey edges, which restricts our ability to detect their satellites. To account for this, we correct the galaxy counts in each annulus by the fraction of the annulus that falls outside of the survey boundaries. The locations of random annuli, and the corrections, are determined in the same way as for the central galaxies. The only other restriction we place on the random fields is that they are not centered within 6 arcsec (about 50 kpc, projected) of any central. We have not required that the random fields have zero overlap with areas around our centrals, as the surface density of our centrals is $\sim 2\,\mathrm{arcmin}^{-2}$, and such a constraint would be too prohibitive. This is a tradeoff between our requirement to subtract off statistically the foreground and background galaxies, and having a sufficiently high number of the random fields to measure the background accurately in each ZFOURGE field. We then subtract the number density of satellites in the random pointings from the number density of satellites of each central. In practice, we measure the number density of galaxies in 100 random pointings and take the average to estimate the number density of foreground and background galaxies for each central in each ZFOURGE field.

Figure 3 shows the raw number density of galaxies measured around both the centrals and measured in random pointings. In each field there is a strong statistical excess of galaxies around our centrals extending from 10 kpc to $\sim$ 100–400 kpc ($\sim$12–50 arcsec), which we attribute to physically associated satellites. There are slight variations in the N_{sat} distribution inferred from the background, as we would expect from natural field-to-field variations. We see no substantial variation in the N_{sat} projected distributions between the three separate fields.

The restriction on the location of the random aperture has little effect on our conclusions. We have tested if this signal changes if we require that no random background aperture is centered within 12 arcsec of a central (compared to the 6 arcsec requirement above), but we find that this does not change significantly the number density of galaxies in the random pointings, and therefore this does not affect our measurement. Similarly, we also find that there is no significant change if we place no restrictions on the locations of the random background apertures.

At smaller projected distances (< 10 kpc), we are unable to measure reliably the number density of satellites, as such objects are blended with the isophotes of the central galaxies. For example, we cross-match our central galaxy catalog from ZFOURGE to the morphology parameter catalog for the CANDELS WFC3/F160W imaging from van der Wel et al. (2012). From this, the typical effective radii of our centrals at $1 < z < 3$ is ~ 3.2 kpc, consistent with measurements of massive galaxies at $z \sim 2$ from van Dokkum et al. (2010). Furthermore, van Dokkum et al. show that such galaxies have $\sim 1\%$ of their stellar mass at a distance of 10 kpc. Therefore, it seems likely that satellites around these galaxies would be indistinguishable from substructure in the centrals for projected distances $r < 10$ kpc. Indeed,

Figure 5. The average projected radial profile of satellites around all central galaxies at $1 < z < 3$ with stellar masses of $\log(M_c/\mathrm{M}_\odot) > 10.48$ (green solid line) combined from all ZFOURGE fields. The radial profile is fitted well with a power-law model with $r^{-1.2}$ (dotted line) and a projected NFW model with $r_s = 61.1 \pm 7.8$ kpc (dashed line) over the range $10 < r/\mathrm{kpc} < 350$.

doing a careful analysis by subtracting the light from the central, Tal et al. (2012) find that the number density of satellites around centrals follows a $r^{1/4}$-law, consistent with the surface-brightness profile of the central galaxies. This suggests that radial density profile of satellites at small scales is strongly influenced by the baryonic content of the central galaxy, rather than the dark matter halo.

Figure 4 shows the number density of satellites measured for the centrals in each ZFOURGE field, and for the combined sample. The satellite distribution in each field is consistent with that measured in the combined sample for $10 < r/\mathrm{kpc} < 100$, and we observe differences at larger and smaller radii. ZFOURGE contains three largely separated fields on the sky, and we interpret the differences at larger radii as a result of field-to-field variations in the number density of background/foreground galaxies in each field.

3.2. Model Fitting

We fit the combined projected number-density profile of satellites using a simple powerlaw model, where $N_{\mathrm{sat}} \propto r^\gamma$. Figure 5 shows that in the range $10 < r/\mathrm{kpc} < 350$ the profile is well described by the power-law with $\gamma = -1.24 \pm 0.04$. The power-law slope of the projected radial profile of satellites around luminous red galaxies at $z = 0.34$ is -1.1 (Tal et al. 2012), which is marginally consistent with our measurement here.

We also compare our measured projected radial profile of satellites with a projected NFW profile, which Bartelmann (1996) show is

$$\Sigma(x) = \begin{cases} (x^2-1)^{-1}\left(1 - \frac{2}{\sqrt{x^2-1}}\arctan\sqrt{\frac{x-1}{x+1}}\right) & (x > 1) \\ 1/3 & (x = 1) \\ (x^2-1)^{-1}\left(1 - \frac{2}{\sqrt{1-x^2}}\mathrm{arctanh}\sqrt{\frac{1-x}{1+x}}\right) & (x < 1) \end{cases}$$

where $x \equiv r/r_s$ and r_s is the NFW-profile scale radius. We utilize the nonlinear least-squares curve fitting program MPFIT (Markwardt 2009) to fit the projected NFW model to the measured projected radial profile of
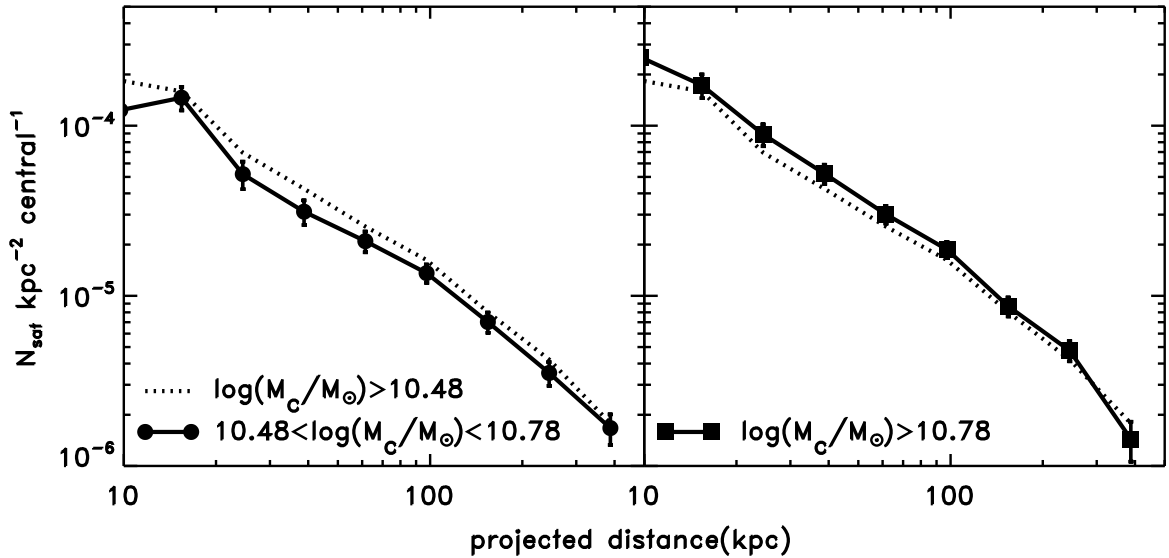
Figure 6. The dependence of the number density of satellites on stellar mass of the central. *Left:* the projected radial profile around all ZFOURGE centrals at $1 < z < 3$ with stellar masses of $10.48 < \log(M_c/M_\odot) < 10.78$ (solid line with circles) compared with that of all samples with stellar masses of $\log(M_c/M_\odot) > 10.48$ (dotted line), *Right:* same as the left panel but for the comparison between the profile of satellites around centrals with stellar masses of $\log(M_c/M_\odot) > 10.78$ (solid line with boxes) and the profile of total centrals. The number of satellites around centrals with stellar masses of $\log(M_c/M_\odot) > 10.78$ is higher on average than that around centrals with stellar masses of $10.48 < \log(M_c/M_\odot) < 10.78$ at 1.9σ.

satellites around centrals at $10 < r/\mathrm{kpc} < 350$, where we fit for both the normalization factor and scale radius.

Figure 5 shows that our derived projected radial density of satellites at $1 < z < 3$ is well fitted by the projected NFW model with $r_s = 61.07 \pm 7.8\,\mathrm{kpc}$. Assuming the scale radius is independent of redshift and only scales with a halo mass as $r_s \sim M_h^{0.45}$ (e.g., Bullock et al. 2001), this would predict $r_s \simeq 200$ kpc at $z = 0$ (assuming a factor ~ 10 growth in halo mass, see e.g.,Moster et al. (2013)). This is smaller than that found by Tal et al. (2012), who find $r_s \sim 270$ kpc for galaxies at $z = 0.02$ in SDSS, but the results are probably consistent as the galaxies in their sample correspond to progenitors with higher stellar masses by factors of ~ 3–5 compared to our sample here (e.g., Tal et al. 2013). Furthermore, this provides us with confidence that our measured satellite distribution is tracing the dark-matter halo of the centrals in our ZFOURGE samples.

4. THE SATELLITE DISTRIBUTION DEPENDENCE ON GALAXY PROPERTY

4.1. *Significance estimation*

It is desirable to assign a significance statistic (p-value) when comparing the differences between the satellite number densities for different subsamples. The uncertainties of each datum of our projected radial distribution of satellites (N_{sat} in the figures above) are derived using simple Poisson statistics. When comparing the satellite number density distributions for difference subsamples, we use two methods, a direct rank-sum test and a Monte Carlo simulation. In practice, for reasons described below we find that the Monte Carlo simulation provides more physical probabilities, and we will use those to estimate the significance in our results.

We first apply a one-sided Wilcoxon-Mann-Whitney rank-sum (WMW) test (Mann & Whitney 1947) to quantify a probability that the number density of satellites around quiescent and star-forming centrals have the

same parent population. The WMW test measures a probability (p-value) using the data and Poisson errors on the satellite distributions between two subsamples (e.g., the quiescent and star-forming centrals). However, the WMW test is not strictly appropriate for our analysis because we are applying it to heavily binned data: each datum is binned (logarithmically) in radius over $10 < r/\mathrm{kpc} < 200$. In particular, the WMW test is insensitive to the fact that our sample includes hundreds of central galaxies and thousands of satellite galaxies.

To estimate meaningful p-values, we use a Monte Carlo approach. We create 10,000 simulations for each subsample of central galaxies. For a given stellar mass range of the central subsample, we randomly select new samples of centrals from the subsample (allowing replacement). We then randomly assign each galaxy to be either quiescent or star-forming. In each simulated subsample, the number of the quiescent and star-forming centrals are equal to the actual number of each in the real subsamples. We then recalculate the radial number density of satellites for each set of random samples and calculate the p_{WMW}–value using the WMW test for each iteration. The likelihood from the Monte Carlo simulations (p_{MC}) are calculated by determining the fraction of the number of simulations when we have the p_{WMW} less than the p_{WMW} value we derive from the real data. A summary of these likelihoods is given in Table 2.

4.2. *Dependence on Central Stellar Mass*

We study how the number density of satellites depends on the stellar mass of centrals by dividing our central galaxy sample into two mass bins: $10.48 < \log(M_c/M_\odot) < 10.78$ and $\log(M_c/M_\odot) > 10.78$. We then recompute the number density of satellites for each of these subsamples using the method above. Figure 6 shows that the more massive centrals have a higher number density of satellites compared to the lower mass centrals. Using our Monte Carlo simulations (see § 4.1), we

find that the significance of this result is $p_{MC} = 0.026$ ($\simeq 1.9\sigma$). Therefore, there is suggestive evidence that the number of satellites increases with the stellar mass of the central galaxy.

4.3. Dependence on Star Formation Activity of Central Galaxy

We investigate how the satellite distribution depends on the star-formation activity of the central galaxies by dividing our sample of central galaxies into subsamples that are star-forming and quiescent (where these labels correspond to galaxies with high and low sSFRs) using their rest-frame $U - V$ and $V - J$ colors as illustrated in Figure 1 and discussed in § 2.1. We then recompute the satellite distribution for each subsample.

Figure 7 shows the projected radial distribution of satellites around the star-forming and quiescent centrals with $\log(M_c/M_\odot) > 10.48$. We find that quiescent centrals host more satellites than their star-forming counterparts. Using our Monte Carlo simulation the likelihood we would obtain this result by chance has a probabilty of $p_{MC} = 0.081$, corresponding to 1.4σ significance.

We further investigate how the number density of satellites depends on both star-formation activity and stellar mass of the central. Figure 8 shows for centrals with moderate stellar mass $10.48 < \log(M_c/M_\odot) < 10.78$. There is no significant evidence that the number density depends on star-formation activity (with a p-value $p_{MC} = 0.478$): both quiescent and star-forming moderate mass centrals have the same number of satellites. In contrast, all the difference in the number density of satellites occurs for centrals at the high stellar-mass end. For the high mass centrals, $\log(M_c/M_\odot) > 10.78$, the quiescent central galaxies have a significant excess of satellites compared to the star-forming centrals, with a p-value of $p_{MC} = 0.002$ (significant at about $\simeq 3.1\sigma$). We discuss the implications of these results in § 5.

4.4. Cumulative Number Density of Satellite Galaxies

We integrate the satellite number densities to measure the total (cumulative) number of satellites within a projected distance of the centrals in our samples down to our mass limit for the satellites, $\log(M/M_\odot) > 9$. Figure 9 compares the cumulative number density of satellites around quiescent centrals and star-forming centrals with $10.48 < \log(M_c/M_\odot) < 10.78$ and $\log(M_c/M_\odot) > 10.78$. On average the intermediate mass centrals have ≈ 1 satellite more massive than $\log(M_{sat}/M_\odot) > 9$ within 100 kpc. This is true for both the star-forming and quiescent centrals. The intermediate mass star-forming galaxies have an excess of satellites at larger projected radii than the quiescent centrals, but this has $<2\sigma$ significance.

Figure 9 also shows that the massive quiescent centrals ($\log(M_c/M_\odot) > 10.78$) have nearly double the number of satellites more massive than $\log(M_{sat}/M_\odot) > 9$ within 100–400 kpc compared to the massive star-forming centrals. On average a massive star-forming central has ≈ 2 such satellites, whereas a massive quiescent central has ≈ 4. These results are comparable with the number of satellites found around massive centrals by Tal et al. (2013), who find that on average the total number of galaxies with the mass ratio of 1:10 and within 400 kpc around the massive centrals between $z = 0.04$ to $z = 1.6$ is 2 to 3.

5. DISCUSSION

5.1. Why do Quiescent and Star-forming Centrals have Different Satellite Distributions?: the Effects of Stellar Mass and Redshift

There is significant evidence that at high stellar mass ($\log(M_c/M_\odot) > 10.78$) quiescent galaxies have more satellites than star-forming galaxies. There are two interpretations. One is that there is something intrinsic to a galaxy being quiescent that also causes the galaxy to have more satellites. The second is that the higher number of satellites is related to stellar mass. If the quiescent centrals have higher stellar masses than the star-forming galaxies—even though the stellar mass *limit* is the same—then they may also be expected to have more satellites.

We test the second of these possibilities by looking at the cumulative stellar mass distribution of the quiescent and star-forming centrals. As shown in Figure 10, indeed the quiescent centrals have a slightly higher median stellar mass, which is higher than the median for the star-forming centrals by 0.05 dex.

Although this difference in stellar mass between the quiescent and star-forming centrals is small, it could affect the number of satellites. Therefore, we make a new sample of quiescent centrals from our real sample. First, we divide the sample of centrals into narrow stellar mass bins. In each stellar mass bin we randomly select equal numbers of quiescent and star-forming galaxies, therefore creating a new sample matched in stellar mass. The numbers of the quiescent and star-forming centrals in the matched stellar mass samples are shown in Table 2. The right panel of Figure 10 shows that the stellar mass distributions of the matched samples agree very well.

After we match the mass distributions of quiescent and star-forming centrals, we then recalculate the number density profiles of satellites around the centrals for each subsample. Figure 11 shows that the number densities of satellites of moderate mass quiescent and star-forming centrals with $10.48 < \log(M_c/M_\odot) < 10.78$ are nearly identical with no evidence for any difference. Our Monte Carlo tests (§ 4.1) give a 98.5% likelihood ($p_{MC} = 0.985$) that the distributions are identical.

However, the excess of satellites around the massive quiescent centrals with $\log(M_c/M_\odot) > 10.78$ compared to the massive star-forming centrals is still significant, where our Monte Carlo tests give a likelihood that we would have obtained this result by chance as 0.4% (i.e., the difference is significant at $\simeq 2.7\sigma$ ($p_{MC} = 0.004$)). Therefore, while the offset in the stellar mass accounts for some of the increase in the number of satellites around the massive centrals, it is unable to account for all of it. Even though the stellar masses are matched, the massive quiescent centrals have more satellites than star-forming centrals.

As another check, one could expect that quiescent and star-forming galaxies may have different redshift distributions, i.e., if at fixed stellar mass the star-forming galaxies lie at higher redshift, then this could possibly affect our results, as the number of satellites (and dark matter halo mass) could build up with time. For example, Moster et al. (2013) show that at fixed stellar mass the halo mass of massive galaxies increases with decreasing redshift.
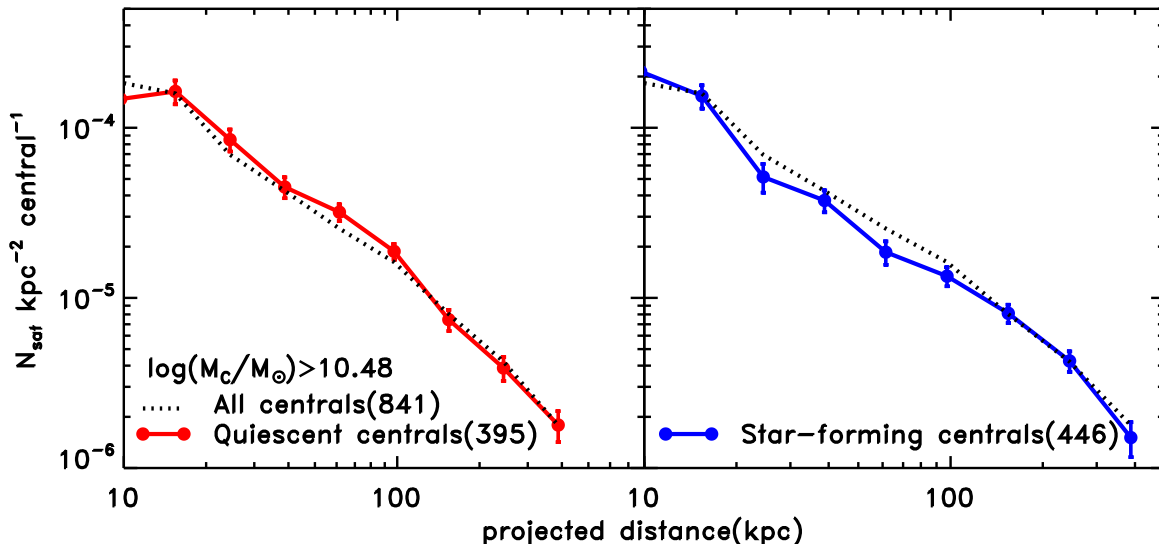
Figure 7. The dependence of the number density of satellites on star-formation activity of the central. *Left:* the projected radial profile around all centrals (black dotted line) at $1 < z < 3$ with stellar masses of $\log(M_{\rm c}/{\rm M}_\odot) > 10.48$ compared with the profile of quiescent centrals (red solid line). *Right:* the projected radial profile around all centrals (black dotted line) at $1 < z < 3$ with stellar masses of $\log(M_{\rm c}/{\rm M}_\odot) > 10.48$ compared with the profile of star-forming centrals (blue solid line). In each panel, the number in parentheses gives the number of centrals in each subsample. The number of satellites around quiescent centrals is higher on average than that around star-forming centrals at 1.4σ.

Figure 12 compares the redshift distributions of quiescent and star-forming centrals for moderate mass and high mass centrals. Using the WMW statistic we find no statistically significant difference between the quiescent/star-forming redshift distributions for moderate mass centrals ($p_{\rm WMW} = 0.46$). The median redshift of quiescent and star-forming centrals are 1.63 and 1.71, respectively. For high-mass centrals the quiescent/star-forming redshift distribution is significantly different ($p_{\rm WMW} = 0.002$). The median redshift of quiescent and star-forming centrals are 1.57 and 1.79, respectively. This difference is not a surprise, as the quiescent fraction of galaxies at fixed mass increases with decreasing redshift.

In order to test whether this difference in redshift distributions affects our results, we match the redshift distributions of high-mass quiescent and star-foming centrals and recalculate the number density profiles of satellites for each subsample. We find that the difference in the redshift distributions does not significantly change our main result: there are still more satellites around massive quiescent centrals compared to their star-forming counterparts.

As a final check, we recalculate the number density of satellites for our samples of centrals, restricting the redshift range of centrals to $1 < z < 2$. The results are consistent with the satellite distribution measured for the full $1 < z < 3$ samples. This also implies that the number of satellites does not change very much over this redshift range. Tal et al. (2013) find that the radial number density of satellites has not evolved much over $z = 0.04 - 1.6$. Therefore, our results show that the trend observed by Tal et al. extends to $z \sim 3$.

To summarize, there appears to be some physical connection between the quenching of star-formation and the presence of an increased number of satellites, at least for massive galaxies. One likely explanation is that the higher number of satellites corresponds to larger dark-matter halo masses, and that at fixed stellar mass the quiescent galaxies have higher halo mass. Because we have no direct measures of the halo masses of the galaxies in our sample, we test this conclusion using semi-analytical models of galaxy formation in the next section.

### 5.2. Comparison to the Guo et al. Semi-Analytic Model: the Role of Halo Mass

To further explore the physical reasons that the massive ($\log(M_{\rm c}/{\rm M}_\odot) > 10.78$) quiescent centrals have more satellites than star-forming counterparts at $1 < z < 3$, we use predictions from the semi-analytic model (SAM) of Guo et al. (2011). The Guo et al. SAM is derived using the Millennium-I simulation (Springel et al. 2001). Henriques et al. (2012) provide mock "lightcone" catalogs from the Guo et al. models, and these lightcones include galaxies at redshifts and to (low) stellar masses comparable to our ZFOURGE dataset.

We select central galaxies from the mock catalogs using the same redshift and stellar mass limits as for our ZFOURGE samples. We further split the mock centrals by sSFR into quiescent ($\log({\rm sSFR/yr}^{-1}) < -10$) and star-forming ($\log({\rm sSFR/yr}^{-1}) > -10$) subsamples. We use the sSFRs for this classification because currently the Henriques et al. (2012) light cones do not include rest-frame magnitudes (e.g., we are unable to classify them using the UVJ colors as done for the ZFOURGE galaxies). However, this makes little difference as Papovich et al. (2012) show that at $z \sim 1.6$ the sSFR threshold of $\log({\rm sSFR/yr}^{-1}) = -10$ effectively separates galaxies classified as quiescent or star-forming by a UVJ-type color-color selection. Therefore, the sSFR selection here is equivalent to our UVJ color-color selection above.

We identify centrals and measure the number density of satellites at $1 < z < 2$ in the SAM lightcone using the same methods as applied to the data. We restrict ourselves to comparisons between the SAM and our data to $1 < z < 2$ and $\log(M/{\rm M}_\odot) > 9.33$ because this is the adopted stellar mass-completeness limit for red satellites
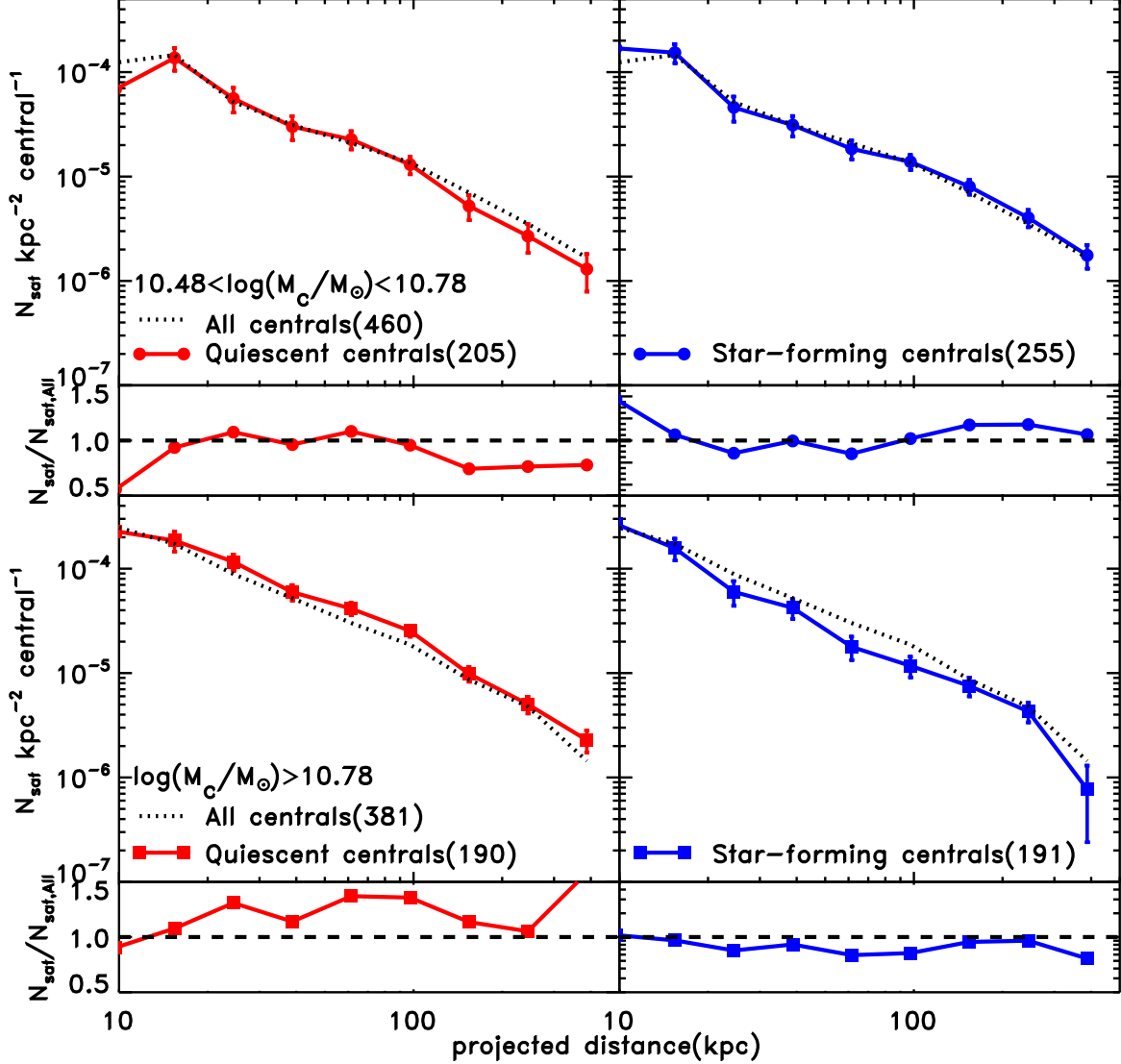
Figure 8. The dependence of the number density of satellites on star-formation activity and stellar mass. *Top:* the projected radial profile around all centrals (black dotted line) at $1 < z < 3$ with stellar masses of $10.48 < \log(M_c/M_\odot) < 10.78$ compared with quiescent centrals (red solid line with circles, left panel) and star-forming centrals (blue solid line with circles, right panel). *Bottom:* the projected radial profile around all centrals (black dotted line) at $1 < z < 3$ with stellar masses of $\log(M_c/M_\odot) > 10.78$ compared with quiescent centrals (red solid line with boxes, left panel) and star-forming galaxies (blue solid line with boxes, right panel). The number in parentheses is the number of centrals in each subsample. Below each N_{sat} plot the ratio of N_{sat} around quiescent (star-forming) centrals to the N_{sat} around all centrals is shown to illustrate the difference between N_{sat} around quiescent and star-forming centrals. The uncertainty on the ratio is derived assuming that the uncertainties on the number of quiescent galaxies and star-forming galaxies both are given by Poisson statistics, and they are uncorrelated. However, the derived error bars of the ratios are very small compared to the size of the data points. For the centrals with stellar masses of $\log(M_c/M_\odot) > 10.78$, the quiescent central galaxies have $\sim 2\times$ the number of satellites compared to star-forming centrals, and this difference is significant at 3.1σ.
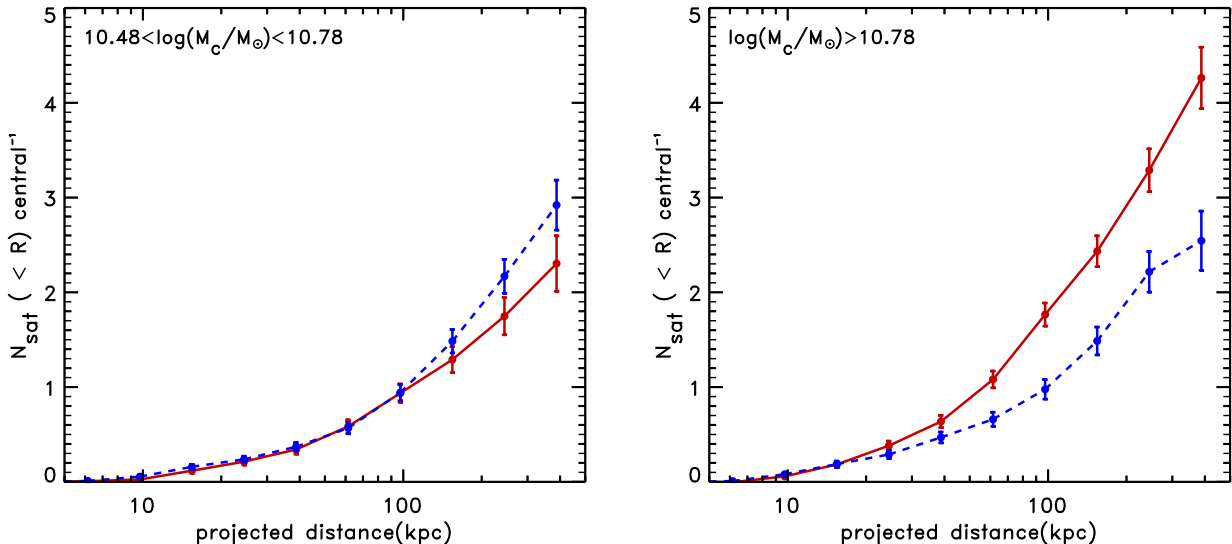
Figure 9. Cumulative number of satellites as a function of projected distance for quiescent central galaxies (red solid lines) and star-forming central galaxies (blue dashed line). *Left:* those centrals with $10.48 < \log(M_c/\mathrm{M_\odot}) < 10.78$. *Right:* the cumulative number of satellites for centrals with stellar mass of $\log(M_c/\mathrm{M_\odot}) > 10.78$. At $1 < z < 3$ centrals with these stellar masses have between 2 and 4 satellites within 400 kpc depending on mass and star-formation activity.
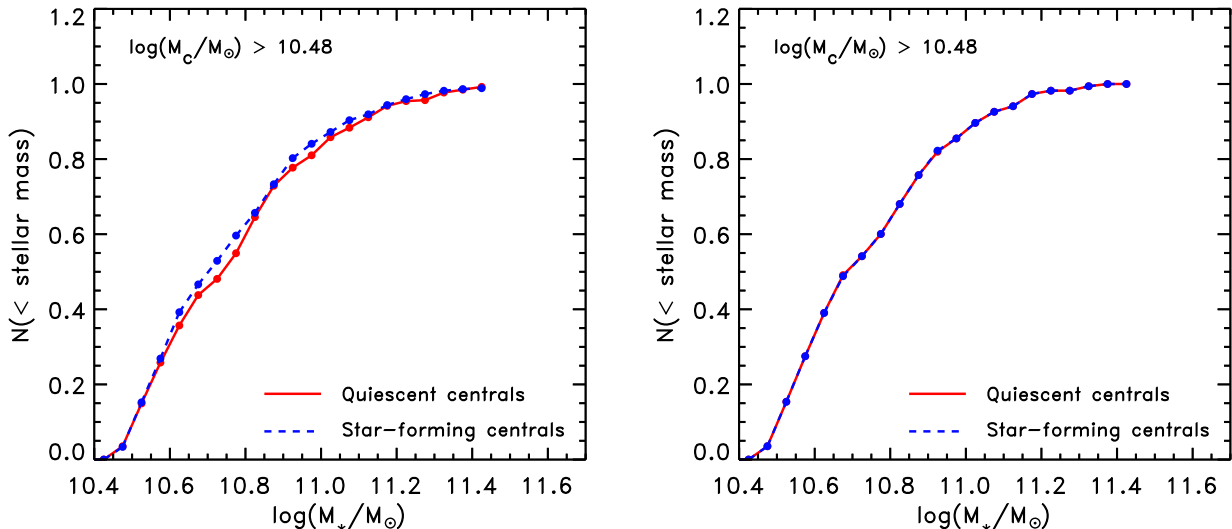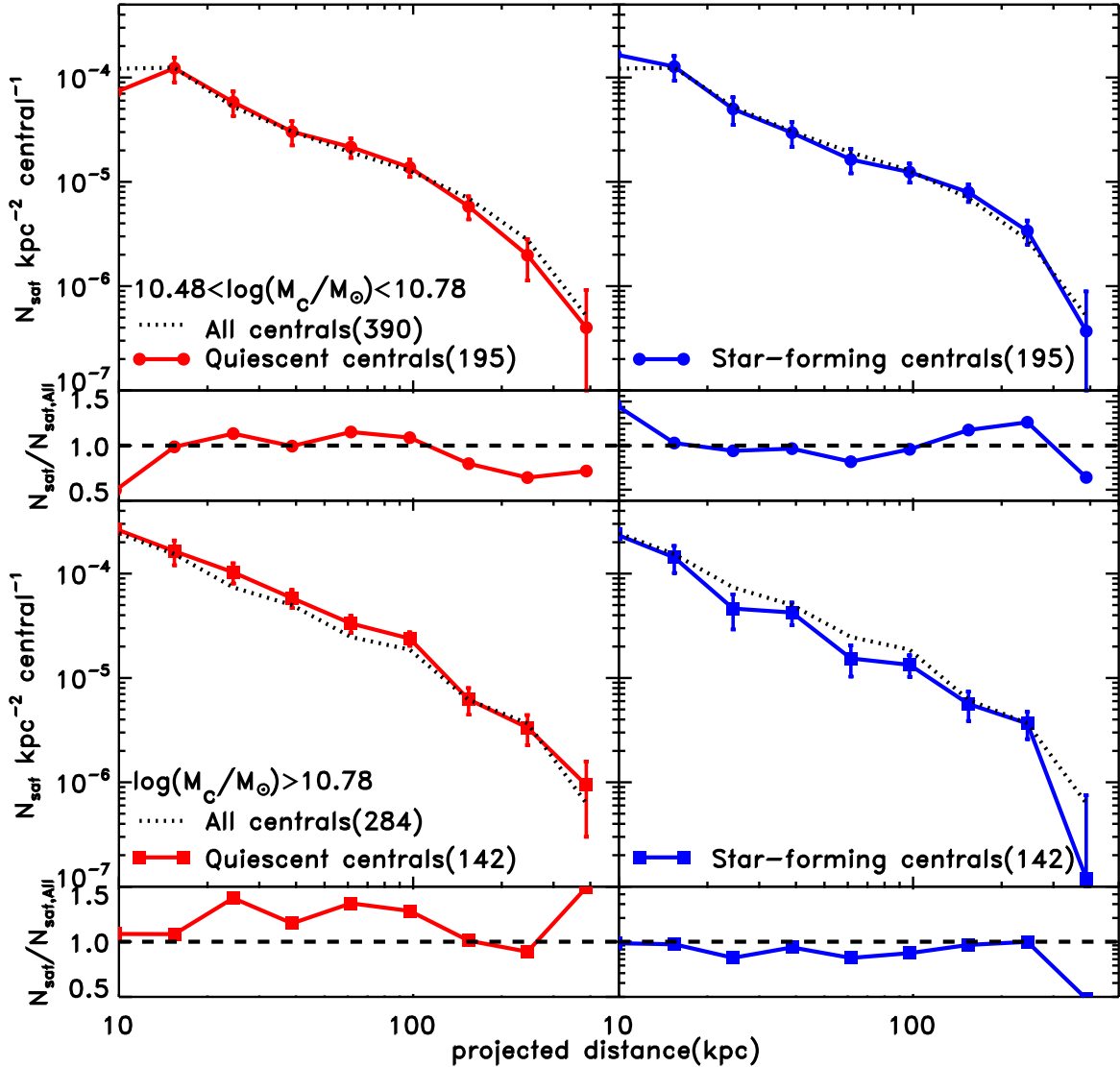

Figure 10. Cumulative distribution in stellar mass for the quiescent centrals (red curves) and star-forming centrals (blue curves), for centrals $\log(M_c/\mathrm{M_\odot}) > 10.48$. *Left:* the stellar mass distribution of the full samples in our ZFOURGE data. The quiescent centrals have a slightly higher median stellar mass, and this could be related to those galaxies having more satellites than the star-forming galaxies. *Right:* the same distribution after we have matched the stellar mass distributions. This allows us to test if the quiescent centrals have more satellites even when they are matched in stellar mass to the star-forming centrals.

at $z = 2$ in the ZFOURGE data (Tomczak et al. 2014). We note that the SAM is also complete to this mass limit. We then measure the projected radial number density of satellites around centrals in the SAM and in the data using this mass limit and redshift range.

Figure 13 compares the satellite number density profiles in the SAM for the different central samples in our ZFOURGE data. The shape of the distributions is similar between the SAM and the data, but the SAM has $\sim 3\times$ the satellites than the data at nearly all projected radii. For our comparison here, we are interested in the relative difference between the quiescent and star-forming centrals in the data and the simulation, so this offset is less important. The reason for this offset is an interesting problem (this is similar to the well-known "missing satellite problem" (Bullock 2010)), and may in-

dicate a mistreatment of important physics in the models. For example, the stellar mass functions in the SAM show a higher number density of lower mass galaxies at $1.3 < z < 3.0$ compared to observations (see Guo et al. 2011, their Figure 23), and it may be expected that such a disagreement would carry over to the satellite population. However, it is interesting that Wang & White (2012); Wang et al. (2014) find a good agreement in the abundance of satellites in the low-redshift SDSS data and in the Guo et al. (2011) SAM, while we find such differences at higher redshift. It is plausible that the higher abundance of low-mass galaxies ($\log(M/\mathrm{M_\odot}) < 9.5$) at $z > 1$ in the Guo et al. model has been resolved by Henriques et al. (2013, see discussion therein). Henriques et al. comment that in the Guo et al. model low-mass galaxies form too early and are thus overabundant at

Figure 11. Same as Figure 8 but for the subsamples in which the cumulative stellar mass distribution of quiescent and star-forming centrals have been matched (see Figure 10). In the high mass subsample $\log(M_c/M_\odot) > 10.78$, quiescent centrals have a higher number density of satellites compared to star-forming counterparts at 2.7σ even when the stellar mass distributions of the quiescent and star-forming galaxies are fixed.

high redshift. Henriques et al. (2013) introduced modifications to the gas reincorporation time-scales and produced an evolving galaxy population which fits observed abundances as a function of stellar mass and luminosity functions up to $z = 3$. This may help resolve the abundance of satellites as well.

We fit the projected NFW profiles to the satellite distributions of the centrals in the SAM and the data (using the restricted redshift range, $1 < z < 2$, and higher stellar mass-completeness limit for the satellites). The fit to the projected NFW profile for the satellite distribution in the SAM gives $r_s = 76.93 \pm 6.42$ kpc. This is in reasonable agreement with the one we measure for the comparable sample in the ZFOURGE data, where the fit gives $r_s = 66.73 \pm 10.69$ kpc (now restricted to the redshift range $1 < z < 2$, which accounts for the differences between r_s derived here an that for the full redshift range in § 3.2).

To compare with the data, we investigate how the number density of satellites around centrals in the SAM de-

pends on stellar mass and star-formation activity. Figure 14 shows the number density of satellites for all the SAM centrals with $\log(M_c/M_\odot) > 10.48$, and for the quiescent and star-forming centrals separately. As with the data, there is an excess of satellites around quiescent galaxies and most of the signal comes from the most massive centrals, with $\log(M_c/M_\odot) > 10.78$: the p-values are $p_{MC} = 0.032$ ($\simeq 1.9\sigma$) and $p_{MC} = 0.001$ ($\simeq 3.7\sigma$) for the centrals with $10.48 < \log(M_c/M_\odot) < 10.78$ and $\log(M_c/M_\odot) > 10.78$, respectively. As with the data, we investigate if the excess of the satellites around the quiescent galaxies is a result of a higher average stellar mass. We therefore match the stellar mass distributions between the star-forming and quiescent centrals in the SAM (see § 5.1). Figure 15 shows the cumulative stellar mass distribution of the SAM centrals after the stellar mass distributions are matched. Figure 14 shows that quiescent centrals in the SAM have a higher number density of satellites compared to the star-forming centrals, even after the stellar mass distribu-
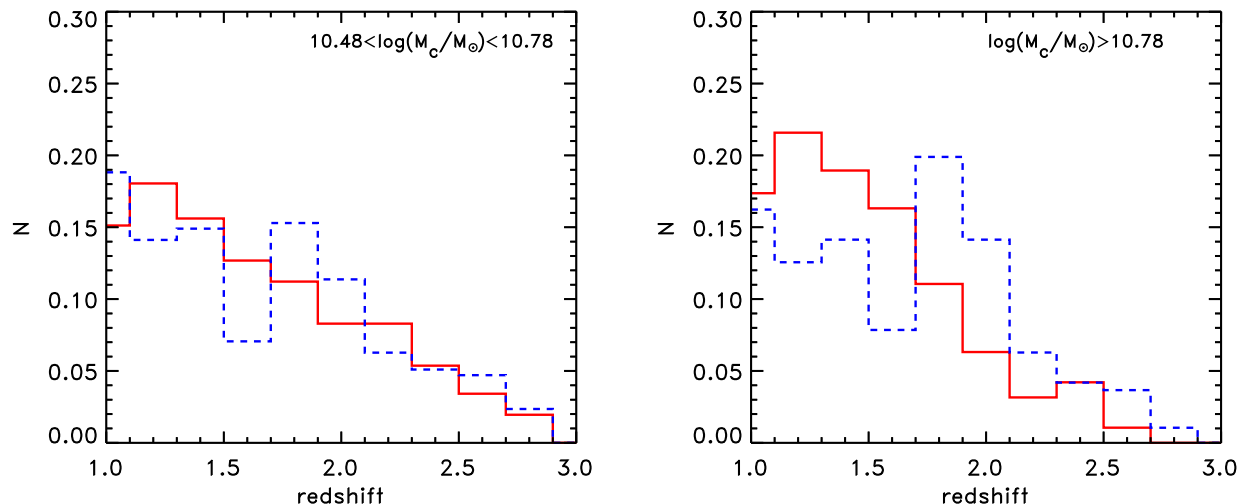
Figure 12. *Left:* The redshift distribution of quiescent (red solid lines) and star-forming centrals (blue dashed lines) at $1 < z < 3$ for intermediate mass, $\log M/M_\odot = 10.48 - 10.78$. There are no statistically significant difference between quiescent/star-forming redshift distribution. *Right:* The redshift distribution of high-mass centrals with $\log M_c/M_\odot > 10.78$. The distribution of star-forming high-mass centrals is shifted toward higher redshift compared to the quiescent high-mass centrals.
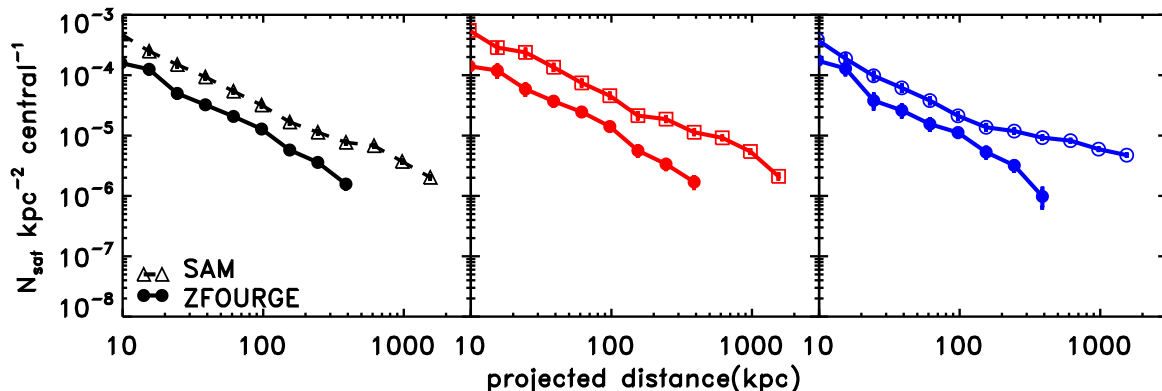
Figure 13. The projected radial profile of satellites around each type of central at $1 < z < 2$ with stellar masses of $\log(M_c/M_\odot) > 10.48$ for centrals selected from the semi-analytic model (SAM; open circles) compared to the satellites around the centrals in our ZFOURGE dataset (filled circles). The left panel shows the satellites for all centrals, the middle panel shows the results for quiescent centrals, and the right panel shows the results for star-forming centrals. In all cases the shape of the satellite distribution is similar for the centrals in the SAM and data, but the normalization is higher for the centrals in the SAM.

tions have been matched. The p-values are $p_{MC} = 0.050$ ($\simeq 1.7\sigma$) and $p_{MC} = 0.016$ ($\simeq 2.1\sigma$) for the centrals with $10.48 < \log(M_c/M_\odot) < 10.78$ and $\log(M_c/M_\odot) > 10.78$, respectively.

The difference in number density of satellites between quiescent and star-forming centrals in the SAM is similar to that observed in our centrals in the ZFOURGE data. The massive quiescent centrals ($\log(M/M_\odot) > 10.78$) have about twice the number of satellites relative to massive star-forming centrals. This is still the case in a stellar mass-matched sample. However, we do note that the difference in satellite content can still be found in the SAM at intermediate masses ($10.48 < \log(M_c/M_\odot) < 10.78$), whereas we do not see a significant difference in the data.

It is a concern that our sample of centrals could have some contamination from galaxies misclassified as centrals that are themselves satellites of other centrals. Since this contamination is expected to be worse at intermediate masses than at higher masses, this may affect our results on the mass-dependence of satellite content. In particular, it could contribute to the lack of observed difference in satellite content between intermediate-mass

quiescent and star-forming galaxies. One way to circumvent the problem of satellite contamination would be to apply isolation criteria for centrals, however this would reduce our sample size[22].

Therefore, to test the magnitude of the effect of satellite contamination in our central samples, we use the mock catalog, in which the true central and satellites are known. We find that $\sim 72\%$ of all galaxies at intermediate mass ($10.48 < \log(M_c/M_\odot) < 10.78$) are centrals, while ($\log(M_c/M_\odot) > 10.78$) $\sim 78\%$ of all galaxies in the high-mass sample are centrals, where the rest are misclassified satellites. We excluded these "false centrals" and recalculated the number density of satellites, again divided into subsamples of quiescent and star-forming centrals. For intermediate-mass centrals, the number of satellites around both quiescent and star-forming galaxies decrease by $\sim 30\%$. Because this affects both subsamples nearly equally it does not change the relative differ-

[22] We also note that isolation criteria can introduce a bias against overdense regions, as discussed by Wang & White (2012) and Wang et al. (2014). This bias is stronger when the signal is weak, i.e. at large distances and for low-mass centrals.
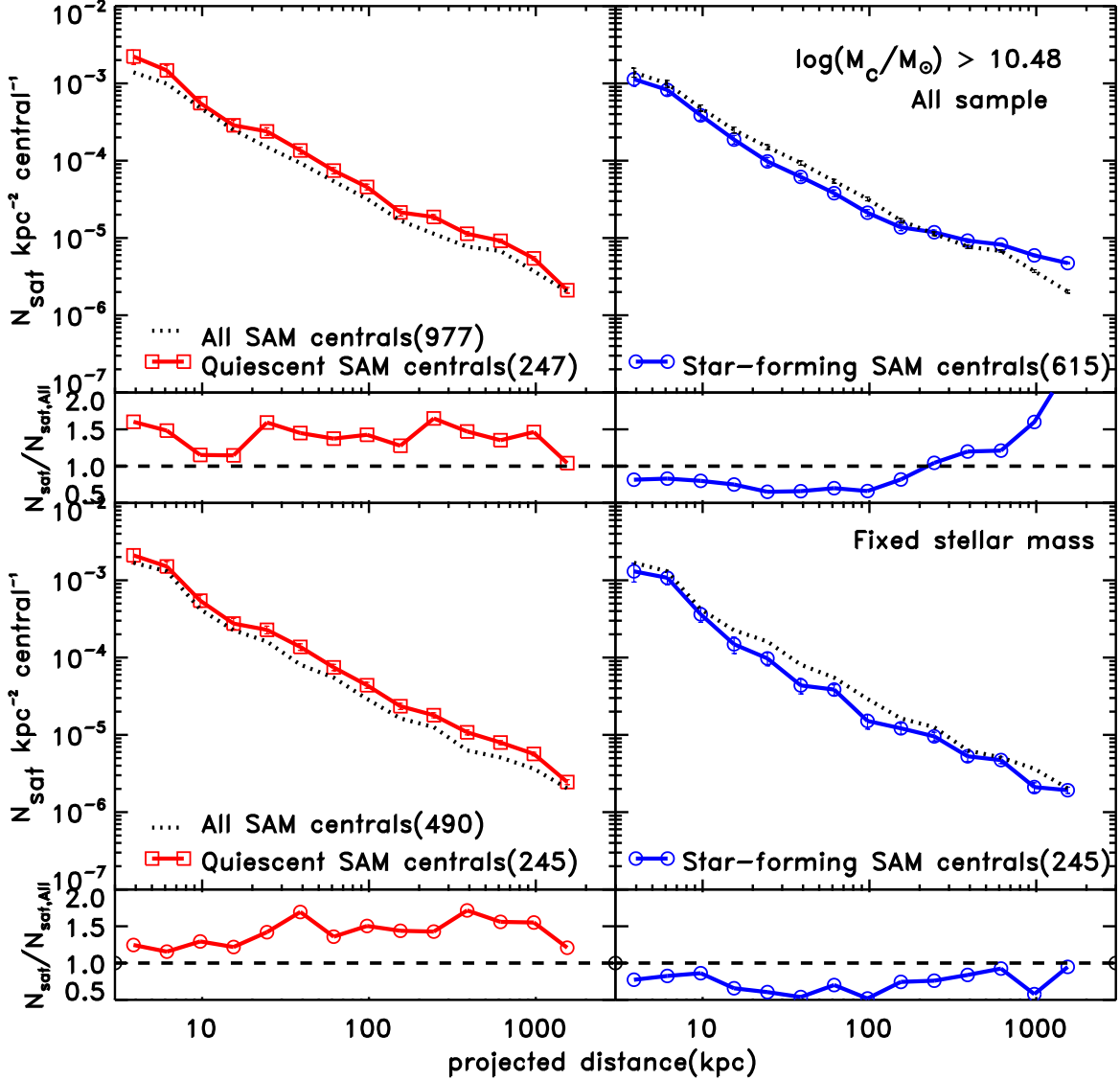
Figure 14. *Top:* the projected radial profile of satellites around all centrals in the SAM (black dotted line), quiescent centrals (red solid line with boxes in the left panel), and star-forming centrals x(blue solid line with filled circles in the right panel) at $1 < z < 2$ with stellar masses of $\log(M_c/M_\odot) > 10.48$. *Bottom:* same plot as the top panels but where we have matched the stellar mass distributions of the quiescent and star-forming centrals. In each panel, the number in parentheses indicates the number of centrals in each subsample. There is a significant excess of satellites around quiescent central even when we match the stellar mass distributions of the centrals.

ence between them, and this should have no impact on our conclusions. For high mass centrals, the number density of satellites declines by $\sim 40\%$ for star-forming centrals, but only by $\sim 10\%$ for quiescent centrals. Therefore, while we make no correction for "false centrals" in our analysis, we note that correcting for this affect would *reduce* the number density of satellites around the high-mass star-forming centrals relative to the high-mass quiescent galaxies, enhancing the significance of difference between these subsamples measured in the data.

Therefore, we use the mock catalog from the SAM to investigate the underlying reason for the excess satellites around massive quiescent galaxies. The main reason appears to be that in the SAM the quiescent centrals have higher halo masses compared to the star-forming centrals at fixed stellar mass. Figure 15 shows that after we have matched the stellar mass distributions of the centrals in the SAM, the quiescent centrals have a higher median halo mass by a factor of ≈ 0.3 dex (factor of order 2).

To test if halo mass is the driving cause, we match the halo mass distributions between the quiescent and star-forming centrals in the SAM using the method to match the stellar mass distributions (see § 5.1). Figure 16 shows the number density of satellites around quiescent and star-forming centrals after matching their halo mass distributions. The difference in the number density of satellites has almost entirely disappeared. Using our p-values from Monte Carlo simulations (see § 4.3), we derive a likelihood of $p_{MC} = 0.176$ ($\simeq 0.9\sigma$) that there is a difference between the satellite distributions for the centrals with $\log(M_c/M_\odot) > 10.48$. Therefore, in the SAM most of the excess in the number density satellites around quiescent galaxies can be attributed to those galaxies having higher halo masses compared to star-forming centrals.

In ΛCDM, the dark matter halos grow through accretion and mergers. Clearly, this will involve the accretion and merging of smaller halos that contain the satellite galaxies. Our analysis of the SAM suggests that
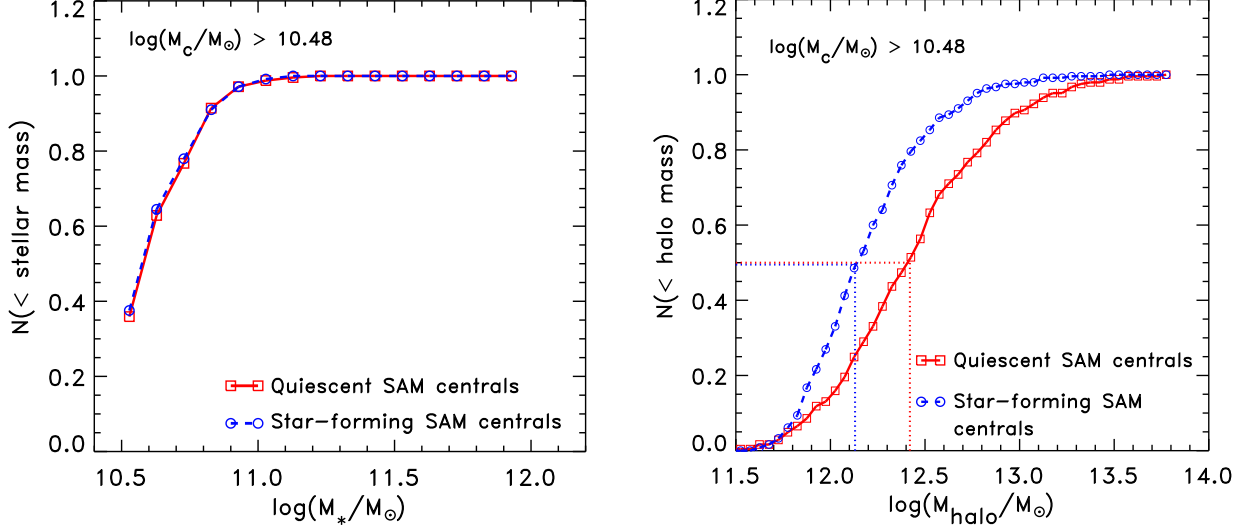
Figure 15. *Left:* the cumulative stellar mass distribution for all quiescent centrals and star-forming centrals in the SAM after matching their stellar mass distributions. *Right:* the cumulative distributions of the halo masses of quiescent (red solid curve) and star-forming (blue dashed curve) centrals after matching their stellar mass distributions (as shown in the left panel). Even when the centrals are matched in stellar mass, the quiescent galaxies have higher halo masses. The dotted lines show that the median halo mass is higher by ≈0.3 dex.
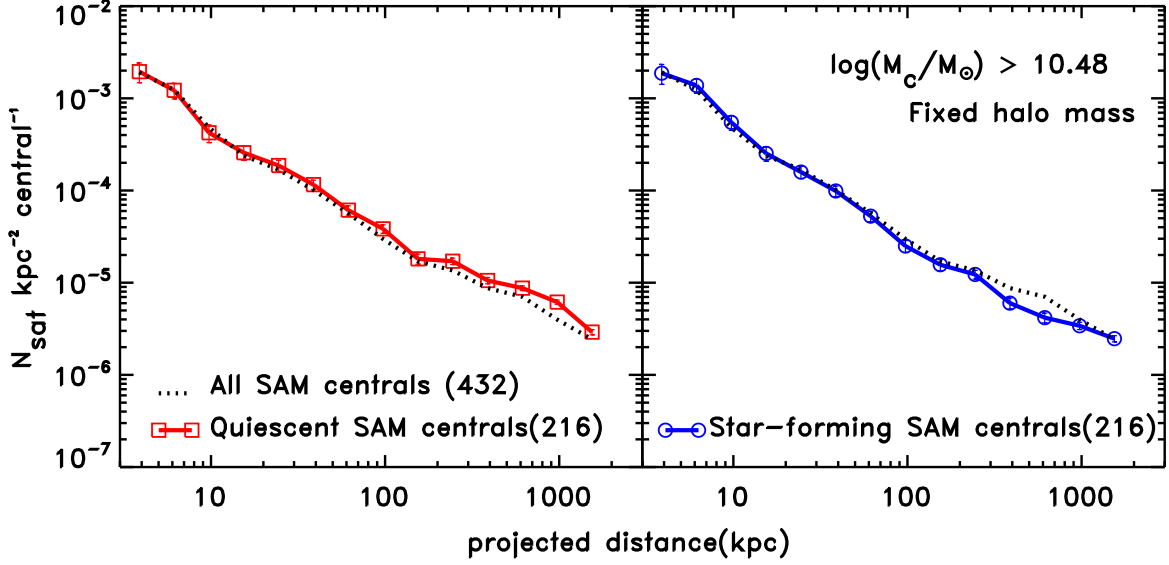
Figure 16. Same as Figure 14 but for the subsamples in which the cumulative halo mass density of quiescent and star-forming centrals in the SAM at $1 < z < 2$ with stellar masses of $\log(M_c/\mathrm{M_\odot}) > 10.48$ have been matched. As indicated in the plot, fixing the halo mass makes the number density of satellites at $10 < r/\mathrm{kpc} < 100$ equal between the star-forming and quiescent centrals. Therefore the excess number density of satellites is an indication that the latter systems have higher halo mass.

the observed difference in satellite content between different types of galaxies is driven by differences in halo mass (see also Cattaneo et al. 2006), with the number of satellites roughly proportional to the halo mass. Therefore, a plausible interpretation of our results is that, at $\log(M_c/\mathrm{M_\odot}) > 10.78$, quiescent centrals have a median halo mass that is about a factor of 2 larger than comparable star-forming galaxies, and that this difference becomes significantly smaller at lower masses.

5.3. *Comparison to Results at Lower Redshift*

Based on our analysis of the simulations in § 5.2, we interpret the excess of satellites around quiescent galaxies as evidence that at fixed stellar mass quiescent centrals have more massive dark matter halos than their star-forming counterparts. Our results are derived from

galaxies from the three fields in ZFOURGE (COSMOS, UDS, CDFS), which are well separated on the sky. We see no evidence for strong field-to-field variance (see § 3.1), and therefore our results seem robust against cosmic variance and/or systematics that vary between the dataset in each field.

Our interpretation that quiescent galaxies have higher dark-matter halos masses compared to star-forming galaxies agrees with findings from analyses of galaxy clustering. These studies also find that quiescent galaxies have stronger clustering amplitudes, and presumably higher dark mass halo masses, compared to their star-forming counterparts (e.g., Li et al. 2006; Hartley et al. 2013). It is perhaps unsurprising that our results agree because our measurement of the number distribution of satellite galaxies is similar to the "one-halo" term of the

galaxy correlation function, but here we measure this to much lower masses and because of our methodology we are able to track the number of satellites and the mass contained within them on average for each central galaxy.

Our results extend trends from the local Universe to higher redshifts. For example, More et al. (2011) study the kinematics of satellite galaxies from SDSS to infer the relation between the properties of central galaxies and their halo masses. Similar to our findings, More et al. conclude that central galaxies with the lower stellar masses ($\log(M/\mathrm{M}_\odot) < 10.8$) have no significant difference in halo mass regardless of being quiescent or star-forming. Moreover, More et al. find that the more massive quiescent centrals have larger halo masses compared to star-forming centrals even when the stellar mass is fixed, again similar to our findings at high redshift. More et al. find that the difference between halo mass of quiescent and star-forming centrals increases from 0.2 to 0.4 dex as the stellar mass of the central increased from $\log(M/\mathrm{M}_\odot) = 10.8$ to $\log(M/\mathrm{M}_\odot) = 11.1$.

These similar results also have been found by other studies of low redshift galaxies using the data from SDSS. Wang & White (2012) study the abundance of satellite galaxies in the stellar mass range $9.0 < \log(M/\mathrm{M}_\odot) < 10.0$. They find that red centrals (what they call "primaries") with the stellar masses of $\log(M/\mathrm{M}_\odot) > 10.8$, have significantly more satellites than blue centrals of the same stellar mass. For the centrals with stellar masses of $\log(M/\mathrm{M}_\odot) \sim 11.2$, red centrals have more satellites about a factor of 2 relative to the star-forming counterparts. They also compare the observation with the Guo et al. (2011) SAMs and find that the red centrals have more satellites because they reside in more massive halos. Recently, Phillips et al. (2014) study the satellites around bright host galaxies with $\log(M/\mathrm{M}_\odot) = 10.5$. The distribution of velocity offset for satellites and their hosts show that at fixed stellar mass the halo mass of passive host galaxies are $\sim 45\%$ more massive than the those of star-forming galaxies.

These results are all in agreement with our findings. Therefore, it seems as if there is little redshift evolution in the conclusion that quiescent galaxies have higher halo masses than star-forming galaxies at fixed stellar mass, at least for the more massive centrals.

5.4. Constraints on Models of Mass Quenching

Qualitatively, it may not be surprising that quenched central galaxies occupy more massive halos than star-forming galaxies at fixed stellar mass, regardless of the particular quenching mechanism. Even after a galaxy stops forming new stars, its halo will continue to grow at a rate comparable to the past average (e.g. Conroy & Wechsler 2009; Moster et al. 2013), meaning that the ratio of dark matter mass to stellar mass will begin increasing relative to galaxies that continue to form stars. This is consistent with the results we derive from the Guo et al. (2011) SAM, where the quiescent galaxies have higher median dark-matter masses compared to the star-forming galaxies, even when we match the stellar mass distributions.

In this respect it is notable that we find a difference in the number of satellites only in our high-mass sample (~ 0.3 dex), and no significant difference at intermediate masses (upper limit ~ 0.1 dex). Using the reasoning

given above, this could be explained if high-mass galaxies quench first, and thus their halos have had the most time to grow relative to their stellar mass. Indeed, such mass–dependent quenching has been clearly demonstrated by Tomczak et al. (2014, see their Figure 11).

Our observations may have interesting implications for the mechanisms that *cause* quenching. It has long been recognized that star formation in high-mass halos may be suppressed due to the shock-heating, and the subsequent inefficient cooling, of infalling gas (e.g. White & Rees 1978; Birnboim & Dekel 2003; Keres et al. 2005; Dekel & Birnboim 2006). Here we wish to interpret our results using a simple model in order to test how halo mass and quenching are related. We first use the redshift-dependent parametrization of the stellar-to-halo mass relation from Moster et al. (2013) to populate halos at $1 < z < 3$ in the Millennium simulation with galaxies, and add in 0.30 dex scatter in stellar mass. We label the galaxies as star-forming if their halo masses fall below a fixed threshold mass (a few times $10^{12}\mathrm{M}_\odot$) and quiescent if their halo masses fall above this threshold (Figure 17, top-left panel). We then calculate the quenched fraction and the average halo mass of star-forming and quiescent galaxies in our two mass bins (Figure 17, top-center and top-right panels, respectively). This fixed halo-mass threshold for quenching results in a quenched fraction that differs significantly between the mass bins, which we do not observe. It also predicts a mean halo mass of quiescent galaxies that is significantly larger than the star-forming galaxies in both stellar mass bins, which we also do not observe.

Because we cannot reproduce the observations for any single value of quenching halo mass and scatter in stellar mass, rather than using the model with a single halo mass quenching, we assign each galaxy a probability for being quenched based on the halo mass. We set the probability to be a steplike function with a soft cutoff profile, $P_{\mathrm{quench}} = 0.5(1 + \mathrm{erf}(\log(M_h/\mathrm{M}_\odot) - \log(M_{0.5}/\mathrm{M}_\odot))/\sigma)$, where erf is the error function[23]. We adjust the parameter $M_{0.5}$, which is defined such that $P_{\mathrm{quench}}(\log(M_{0.5}/\mathrm{M}_\odot)) = 0.5$, and the parameter σ, as well as the scatter in stellar mass to roughly reproduce the observed quenched fraction and the difference in mean halo mass. We find that a $\log(M_{0.5}/\mathrm{M}_\odot)$ of $12.3 - 12.5$, a standard deviation of $0.7 - 0.9$, which corresponds to $P_{\mathrm{quench}} = 0$ for $\log(M_h/\mathrm{M}_\odot) \sim 11 - 11.5$ and $P_{\mathrm{quench}} = 1$ for $\log(M_h/\mathrm{M}_\odot) \sim 13.5$, and a scatter in stellar mass of $0.15 - 0.2$ dex, is able to roughly reproduce the observed quiescent fractions and the difference in the average halo mass of centrals at both stellar mass bins (Figure 17, bottom row). We find that the differences in mean halo mass of quiescent and star-forming galaxies are ~ 0.1 dex and ~ 0.2 dex for intermediate and high stellar mass bins, respectively (Figure 17, bottom right panel), in better agreement with the observations. The small scatter favored by the model in the stellar-to-halo mass relation is due to the fact that we see significant differences in N_{sat} over a relatively small range in stellar mass: the mean mass in the intermediate-mass sample

---

[23] Our choice of functional form for P_{quench} here is arbitrary except that it obeys our requirement that P_{quench} increase with mass. We expect other parameterizations with a mass-dependent P_{quench} can reproduce the data as well.
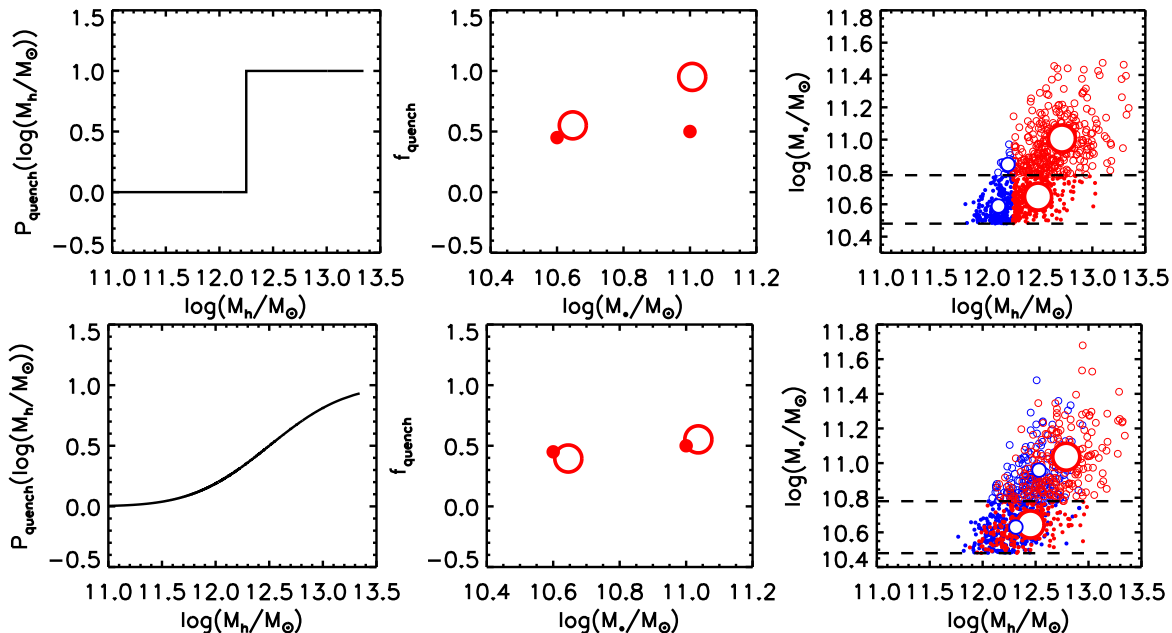
Figure 17. A toy model that explores scenarios in which the quenching of star formation is related to halo mass, and which attempts to explain the large inferred difference in halo mass between star-forming and quiescent galaxies at high stellar masses, while maintaining a smaller difference at intermediate stellar masses. We use the redshift-dependent stellar-to-halo mass relation from Moster et al. (2013) to populate halos from an N-body simulation with galaxies, and add in additional scatter to the stellar masses. We then quench some subset of the galaxies based on their halo mass. *Top:* A scenario where the quenching probability is a step function in halo mass, with a threshold of $\log(M_h/\mathrm{M_\odot}) = 12.25$, as shown on the left. The center panel shows that the predicted quenched fraction in our two stellar mass bins (large open circles) does not agree with the observations (small filled circles). The right panel shows the stellar and halo masses of the simulated galaxies, color-coded according to whether the galaxies have been quenched. The small and large open circles show the mean stellar and halo masses for star-forming galaxies and quiescent galaxies, respectively. The mean halo masses differ by 0.3 dex in the intermediate mass bin and 0.5 dex in the high-mass bin, in contrast with the differences inferred from the data, which are ~ 0.08 and ~ 0.3 dex, respectively. *Bottom:* same as the top panels for a scenario where the probability of each galaxy being quenched is modeled as a steplike function with a softened profile. The predicted quenched fractions, and the predicted differences in halo masses between star-forming and quiescent galaxies in our two mass bins, are in significantly better agreement with the data.

is $\log(M_*/\mathrm{M_\odot}) \sim 10.6$, while in the high mass sample it is $\log(M_*/\mathrm{M_\odot}) \sim 11.0$, and so a large amount of scatter would wash out differences in halo mass over this relatively limited range in stellar mass. We do note that the scatter in our modeling represents intrinsic scatter in the stellar-to-halo mass relation *combined with* the random errors in our stellar mass estimates, suggesting that the *intrinsic* scatter must be small indeed.

Our model is simplistic, it is obviously possible to develop it further. For instance, we note that adding a mass-dependent scatter in the stellar masses — where the scatter increases from 0.15 dex at lower masses to 0.3 dex at the higher masses — improves the agreement between the toy model and the data. However, given the uncertainties involved in the current data, particularly with regard to the incompleteness in satellite detection at low masses and the (limited) expected misclassification between centrals and satellites (see § 2.2), our modeling results can only be regarded as indicative, and we do not push the modeling any further.

If our observation that intermediate mass quiescent and star-forming centrals have the same N_{sat} is correct, then our toy model strongly favors a scenario where there is no single quenching halo mass threshold: even at relatively high halo masses ($\log(M/h^{-1}\mathrm{M_\odot}) \sim 12$ based on the SAM), only about 50% of the galaxies are quiescent while the rest remain star-forming, and galaxies have some likelihood of being quenched over a very wide range in halo masses ($\log(M_h/\mathrm{M_\odot}) \sim 11 - 13.5$). One remaining question is that if halo mass quenching is

an important mechanism, *why* do some galaxies remain star-forming while others quench? Our result implies that halo mass can only be a contributing factor. Other factors may include environmental processes (assembly bias and environmental effects on the gas-accretion process), stochastic processes such as mergers, and galaxy structure (e.g Gao et al. 2005; Wechsler et al. 2006; Croton et al. 2007; Cooper et al. 2010; Papovich et al. 2012; Rudnick et al. 2012; Bassett et al. 2013; Lotz et al. 2013).

This result may be expected on theoretical grounds, as some variation in the quenching mass is expected due to variations in metallicity and perhaps also due to the enhanced ability of cold flows to penetrate halos at the higher redshifts in our sample (Dekel & Birnboim 2006; Dekel et al. 2009). A variation in halo mass is also expected based on the results of Gabor & Davé (2012). In their model galaxy quenching is based on the hot gas content of halos, which is correlated with, but not directly tied to halo mass. Recently, Lu et al. (2013) also show that galaxy models require a quenching probability that increases with mass to explain the color-mass distributions of galaxies in the CANDELS survey.

The mergers that grow massive quiescent galaxies are supposed to be primarily dissipationless, and devoid of cold gas available for star-formation (e.g., so-called "dry" mergers, van Dokkum et al. 2010; Oser et al. 2010, 2012; Hopkins et al. 2010). If this is the case, it is expected that satellites around the quiescent centrals in our sample, which will eventually merge with their central galax-

ies, should be largely devoid of gas (or some process must cause them to expel or consume their gas prior to merging with the central). Therefore it may be expected that the satellites should show signs of passive colors. A discussion of the color and stellar mass distributions of the satellites is beyond the scope of the present work, but we will study these distributions in a future paper.

6. SUMMARY

We have studied the statistical distribution of satellites around star-forming and quiescent central galaxies at $1 < z < 3$ using imaging from ZFOURGE and CANDELS. The deep near-IR data allow us to select satellites down to $\log(M/\mathrm{M}_\odot) > 9$ at $z < 3$. The main conclusions of this work are the following.

- The projected radial number density of satellites around centrals with stellar mass $\log(M/\mathrm{M}_\odot) > 10.48$ is consistent with a projected NFW profile.

- We find that the number density of satellites depends on the stellar mass of the central galaxies. The most massive central galaxies ($\log(M/\mathrm{M}_\odot) > 10.78$) have ~ 1.9 times the number of satellites within 400 kpc compared to intermediate mass centrals ($10.48 < \log(M_{\mathrm{c}}/\mathrm{M}_\odot) < 10.78$), which is significant at $\simeq 1.9\sigma$.

- For the most massive galaxies, $\log(M/\mathrm{M}_\odot) > 10.78$, quiescent centrals have ~ 2 times the number of satellites within 400 kpc compared to star-forming centrals (significant at $\simeq 3.1\sigma$). This excess persists at 2.7 sigma significance even when we account for differences in the centrals' stellar mass distributions. In contrast, we find no significant difference in the satellite distributions of less-massive quiescent and star-forming centrals, $10.48 < \log(M/\mathrm{M}_\odot) < 10.78$.

- We interpret the number density of satellites in our data using the semi-analytic model of Guo et al. (2011) from the lightcone made available by Henriques et al. (2012). We find that quiescent galaxies in the model also have more satellites than star-forming galaxies of similar stellar mass. By matching the halo masses of the star-forming and quiescent samples, we demonstrate that the difference in satellite content in the simulation is due almost entirely to differences in halo mass. We interpret this as evidence that the differences in satellite content observed in the data is driven by a difference in halo mass, and conclude that at stellar masses $\log(M/\mathrm{M}_\odot) > 10.78$ the halos that host quiescent galaxies are ~ 0.3 dex more massive than the halos that host star-forming galaxies.

- We use a simple model to investigate the relationship between quenching and halo mass, which roughly reproduces the observed quenched fractions and the differences in halo mass between star-forming and quenched galaxies in our two stellar mass bins. The model suggests a scenario where galaxies have some probability of being quenched over roughly two decades in halo mass,

$\log(M_h/\mathrm{M}_\odot) \sim 11 - 13.5$, where the probability increases with mass. This wide mass range suggests that, while halo mass quenching may be an important mechanism at $1 < z < 3$, halo mass is not the only factor driving quiescence. It remains unclear why some central galaxies in relatively massive halos can keep forming stars.

REFERENCES

Bartelmann, M. 1996, Astronomy and Astrophysics

Bassett, R., Papovich, C., Lotz, J. M., et al. 2013, The Astrophysical Journal, 770, 58

Behroozi, P. S., Conroy, C., & Wechsler, R. H. 2010, The Astrophysical Journal, 717, 379

Bell, E. F., Wolf, C., Meisenheimer, K., et al. 2004, The Astrophysical Journal, 608, 752

Bertin, E., & Arnouts, S. 1996, Astronomy and Astrophysics Supplement

Birnboim, Y., & Dekel, A. 2003, Monthly Notices of the Royal Astronomical Society, 345, 349

Blanton, M. R. 2006, The Astrophysical Journal, 648, 268

Brammer, G. B., van Dokkum, P. G., & Coppi, P. 2008, The Astrophysical Journal, 686, 1503

Bruzual, G., & Charlot, S. 2003, Monthly Notices of the Royal Astronomical Society, 344, 1000

Bullock, J. 2010, eprint arXiv:1009.4505

Bullock, J. S., Kolatt, T. S., Sigad, Y., et al. 2001, Monthly Notices of the Royal Astronomical Society, 321, 559

Capak, P., Aussel, H., Ajiki, M., et al. 2007, The Astrophysical Journal Supplement Series, 172, 99

Cattaneo, A., Dekel, A., Devriendt, J., Guiderdoni, B., & Blaizot, J. 2006, Monthly Notices of the Royal Astronomical Society, 370, 1651

Chabrier, G. 2003, Publications of the Astronomical Society of the Pacific, 115, 763

Conroy, C., & Wechsler, R. H. 2009, The Astrophysical Journal, 696, 620

Cooper, M. C., Gallazzi, A., Newman, J. A., & Yan, R. 2010, Monthly Notices of the Royal Astronomical Society, 402, 1942

Croton, D. J., Gao, L., & White, S. D. M. 2007, Monthly Notices of the Royal Astronomical Society, 374, 1303

Croton, D. J., Springel, V., White, S. D. M., et al. 2006, Monthly Notices of the Royal Astronomical Society, 365, 11

Dekel, A., & Birnboim, Y. 2006, Monthly Notices of the Royal Astronomical Society, 368, 2

Dekel, A., Birnboim, Y., Engel, G., et al. 2009, Nature, 457, 451

Drory, N., Bundy, K., Leauthaud, A., et al. 2009, The Astrophysical Journal, 707, 1595

Fioc, M., & Rocca-Volmerange, B. 1997, Astronomy and Astrophysics

Gabor, J. M., & Davé, R. 2012, Monthly Notices of the Royal Astronomical Society, 427, 1816

Gao, L., Springel, V., & White, S. D. M. 2005, Monthly Notices of the Royal Astronomical Society: Letters, 363, L66

Gavazzi, R., Treu, T., Rhodes, J. D., et al. 2007, The Astrophysical Journal, 667, 176

Giacconi, R., Zirm, A., Wang, J., et al. 2002, The Astrophysical Journal Supplement Series, 139, 369

Greene, J. E., Murphy, J. D., Comerford, J. M., Gebhardt, K., & Adams, J. J. 2012, The Astrophysical Journal, 750, 32

Greene, J. E., Murphy, J. D., Graves, G. J., et al. 2013, The Astrophysical Journal, 776, 64

Grogin, N. A., Kocevski, D. D., Faber, S. M., et al. 2011, The Astrophysical Journal Supplement Series, 197, 35

Guo, Q., White, S., Boylan-Kolchin, M., et al. 2011, Monthly Notices of the Royal Astronomical Society, 413, 101

Hartley, W., Conselice, C., Mortlock, A., Foucaud, S., & Simpson, C. 2014, eprint arXiv:1406.6058

Hartley, W. G., Almaini, O., Cirasuolo, M., et al. 2010, Monthly Notices of the Royal Astronomical Society, 407, 1212

Hartley, W. G., Almaini, O., Mortlock, A., et al. 2013, Monthly Notices of the Royal Astronomical Society, 431, 3045

Henriques, B. M. B., White, S. D. M., Lemson, G., et al. 2012, Monthly Notices of the Royal Astronomical Society, 421, 2904

Henriques, B. M. B., White, S. D. M., Thomas, P. A., et al. 2013, Monthly Notices of the Royal Astronomical Society, 431, 3373

Hilz, M., Naab, T., & Ostriker, J. P. 2013, Monthly Notices of the Royal Astronomical Society, 429, 2924

Hopkins, P. F., Bundy, K., Hernquist, L., Wuyts, S., & Cox, T. J. 2010, Monthly Notices of the Royal Astronomical Society, 401, 1099

Keres, D., Katz, N., Weinberg, D. H., & Dave, R. 2005, Monthly Notices of the Royal Astronomical Society, 363, 2

Koekemoer, A. M., Faber, S. M., Ferguson, H. C., et al. 2011, The Astrophysical Journal Supplement Series, 197, 36

Kriek, M., van Dokkum, P. G., Labbé, I., et al. 2009, The Astrophysical Journal, 700, 221

Lawrence, A., Warren, S. J., Almaini, O., et al. 2007, Monthly Notices of the Royal Astronomical Society, 379, 1599

Li, C., Kauffmann, G., Jing, Y. P., et al. 2006, Monthly Notices of the Royal Astronomical Society, 368, 21

Lotz, J. M., Papovich, C., Faber, S. M., et al. 2013, The Astrophysical Journal, 773, 154

Lu, Y., Wechsler, R. H., Somerville, R. S., et al. 2013, eprint arXiv:1312.3233

Madore, B. F., Freedman, W. L., & Bothun, G. D. 2004, The Astrophysical Journal, 607, 810

Mandelbaum, R., Seljak, U., Kauffmann, G., Hirata, C. M., & Brinkmann, J. 2006, Monthly Notices of the Royal Astronomical Society, 368, 715

Mann, H. B., & Whitney, D. R. 1947, The Annals of Mathematical Statistics, 18, 50

Maraston, C. 2005, Monthly Notices of the Royal Astronomical Society, 362, 799

Marchesini, D., Muzzin, A., Stefanon, M., et al. 2014, eprint arXiv:1402.0003

Markwardt, C. B. 2009, Astronomical Data Analysis Software and Systems XVIII ASP Conference Series, 411

Martig, M., Bournaud, F., Teyssier, R., & Dekel, A. 2009, The Astrophysical Journal, 707, 250

Martin, D. C., Wyder, T. K., Schiminovich, D., et al. 2007, The Astrophysical Journal Supplement Series, 173, 342

Masjedi, M., Hogg, D. W., Cool, R. J., et al. 2006, The Astrophysical Journal, 644, 54

McLure, R. J., Pearce, H. J., Dunlop, J. S., et al. 2012, Monthly Notices of the Royal Astronomical Society, 428, 1088

More, S., van den Bosch, F. C., Cacciato, M., et al. 2011, Monthly Notices of the Royal Astronomical Society, 410, 210

Moster, B. P., Naab, T., & White, S. D. M. 2013, Monthly Notices of the Royal Astronomical Society, 428, 3121

Naab, T., Johansson, P. H., & Ostriker, J. P. 2009, The Astrophysical Journal, 699, L178

Naab, T., Johansson, P. H., Ostriker, J. P., & Efstathiou, G. 2007, The Astrophysical Journal, 658, 710

Nierenberg, A. M., Auger, M. W., Treu, T., Marshall, P. J., & Fassnacht, C. D. 2011, The Astrophysical Journal, 731, 44

Nierenberg, A. M., Auger, M. W., Treu, T., et al. 2012, The Astrophysical Journal, 752, 99

Noeske, K. G., Weiner, B. J., Faber, S. M., et al. 2007, The Astrophysical Journal, 660, L43

Oser, L., Naab, T., Ostriker, J. P., & Johansson, P. H. 2012, The Astrophysical Journal, 744, 63

Oser, L., Ostriker, J. P., Naab, T., Johansson, P. H., & Burkert, A. 2010, The Astrophysical Journal, 725, 2312

Papovich, C., Moustakas, L. A., Dickinson, M., et al. 2006, The Astrophysical Journal, 640, 92

Papovich, C., Bassett, R., Lotz, J. M., et al. 2012, The Astrophysical Journal, 750, 93

Phillips, J. I., Wheeler, C., Boylan-Kolchin, M., et al. 2014, Monthly Notices of the Royal Astronomical Society, 437, 1930

Quadri, R. F., & Williams, R. J. 2010, The Astrophysical Journal, 725, 794

Rudnick, G. H., Tran, K.-V., Papovich, C., Momcheva, I., & Willmer, C. 2012, The Astrophysical Journal, 755, 14

Spitler, L. R., Labbé, I., Glazebrook, K., et al. 2012, The Astrophysical Journal, 748, L21

Springel, V., White, S. D. M., Tormen, G., & Kauffmann, G. 2001, Monthly Notices of the Royal Astronomical Society, 328, 726

Straatman, C. M. S., Labbé, I., Spitler, L. R., et al. 2014, The Astrophysical Journal, 783, L14

Tal, T., van Dokkum, P. G., Franx, M., et al. 2013, The Astrophysical Journal, 769, 31

Tal, T., Wake, D. A., & van Dokkum, P. G. 2012, The Astrophysical Journal, 751, L5

Tilvi, V., Papovich, C., Tran, K.-V. H., et al. 2013, The Astrophysical Journal, 768, 56

Tomczak, A. R., Quadri, R. F., Tran, K.-V. H., et al. 2014, The Astrophysical Journal, 783, 85

Vader, J. P., & Sandage, A. 1991, The Astrophysical Journal, 379, L1

van der Wel, A., Bell, E. F., Häussler, B., et al. 2012, The Astrophysical Journal Supplement Series, 203, 24

van Dokkum, P. G., Whitaker, K. E., Brammer, G., et al. 2010, The Astrophysical Journal, 709, 1018

Wake, D. A., Sheth, R. K., Nichol, R. C., et al. 2008, Monthly Notices of the Royal Astronomical Society, 387, 1045

Wang, W., Sales, L., Henriques, B., & White, S. 2014, eprint arXiv:1403.2409

Wang, W., & White, S. D. M. 2012, Monthly Notices of the Royal Astronomical Society, 424, 2574

Watson, D. F., Berlind, A. A., McBride, C. K., Hogg, D. W., & Jiang, T. 2012, The Astrophysical Journal, 749, 83

Wechsler, R. H., Zentner, A. R., Bullock, J. S., Kravtsov, A. V., & Allgood, B. 2006, The Astrophysical Journal, 652, 71

Whitaker, K. E., Labbé, I., van Dokkum, P. G., et al. 2011, The Astrophysical Journal, 735, 86

White, S. D. M., & Rees, M. J. 1978, Monthly Notices of the Royal Astronomical Society, 183, 341

Williams, R. J., Quadri, R. F., Franx, M., van Dokkum, P., & Labbé, I. 2009, The Astrophysical Journal, 691, 1879

Zehavi, I., Blanton, M. R., Frieman, J. A., et al. 2002, The Astrophysical Journal, 571, 172